AN ABSTRACT OF THE THESIS OF

Phyllis J. Stabeno for the degree of Doctor of Philosophy in Oceanography presented on May 29, 1982

Title: THE REFLECTION, TRANSMISSION AND SCATTERING OF INTERNAL WAVES AT OCEAN FRONTS

Redacted for privacy

Abstract approved: Pearn P. Niiler

A theoretical model of the reflection, transmission, scattering and production of internal gravity wave energy at an idealized front is developed. Two models, one consisting of two and the other of three layers, are examined. Slanting upwards the interfaces between the layers form a frontal structure, and within the frontal region there is a horizontally-sheared, geostrophic velocity. For normally incident waves, a WKB solution is obtained, showing that for sufficiently small wavelengths (relative to the frontal width) virtually all the energy is transmitted through the front without being scattered into other modes. The opposite is true for long waves. Here, if the depth change across the front is large, most of the energy

of a normally incident wave is reflected or scattered into other modes.

A two layer model for waves that are not necessarily normally incident is solved numerically. Along a curve of constant frequency the minimum reflection occurs for waves that are slightly skewed from normal incidence, while the fraction of energy reflected increases as the waves travel more parallel to the front. When critical layers occur , energy can be exchanged between the geostrophic flow and the internal waves. For the frontal shapes considered in this paper, energy is usually gained by the internal wave field at the expense of the mean flow. When there is no critical layer, the Reynolds stress is invariant in the across front direction. When they do occur, the Reynolds stress is not necessarily invariant and is a measure of the amount of energy exchanged between the frontal structure and the internal wave field.

The Reflection, Transmission and Scattering of Internal Waves at Ocean Fronts

by

Phyllis Jean Stabeno

A THESIS

submitted to

Oregon State University

in partial fulfillment of
the requirements for the
degree of

Doctor of Philosophy

Completed April 28, 1982

Commencement June 1982

APPROVED:

Redacted for privacy

Professor of Oceanography
in charge of major

Redacted for privacy

Dean of the School of Oceanography

Redacted for privacy

Dean of Graduate School

Date thesis is presented April 29, 1982

Typed by Jody Shively for Phyllis J. Stabeno

ACKNOWLEDGEMENTS

My grateful appreciation to all those who served on my committe for their suggestions and advice. I thank, especially, my major professor, Dr. P. P. Niiler, and Dr. Roland DeSzoeke for their encouragement and their gifts of time and ideas. Funding for this research was under contract of Office of Naval Research Nooo14-79-C-0004 at OSU.

To my parents for their support and understanding throughout my university career. To all my friends, but especially Rick and Alanna, who helped keep it all in perspective. And to my husband, Mick Spillane, for his love, encouragement and assistance.

TABLE OF CONTENTS

I	Introduction	1
II	The Two Layer Model with Normal Incidence	4
	2.1 Formulation of Problem	4
	2.2 Energy Equation	13
	2.3 Solutions	16
	2.4 Discussion of Solutions	23
III	Two Layer Model with Non-normal Incidence	33
	3.1 The Model	33
	3.2 Matrix Representation	38
	3.3 Matching Conditions	43
	3.4 Energy Equation	47
	3.5 Solutions without Critical Layers	50
	3.6 Solutions with Critical Layers	65
IV	Three Layer Model with Normal Incidence	86
	4.1 Formulation of the Problem	86
	4.2 Modal Structure	91
	4.3 Non-dimensionalization	93
	4.4 Matching Conditions	94
	4.5 Energy Equation	96
	4.6 Solutions and Discussion	97
V	Summary and Conclusions	115

Bibliography 119

Appendix A 121

Appendix B 127

Appendix C 129

LIST OF FIGURES

Figure		Page
1	Schematic representation of the frontal profile.	5
2	Comparison of the two perturbation solutions with the numerical solution for $\alpha_1 = .80$ and $\alpha_2 = .16$.	26
3a	Shape of the frontal interface for three values of α_1, α_2: (a) $\alpha_1 = .80$, $\alpha_2 = .16$; (b) $\alpha_1 = .50$, $\alpha_2 = .10$; (c) $\alpha_1 = .20$, $\alpha_2 = .04$.	27
3b	The fractional reflected energy for the three frontal profiles shown in figure 3a.	28
4	Schematic of the x-y plane, for waves that are not necessarily normally incident upon the front.	37
5	Sketch of the dispersion relationship for ℓ and ℓ' as a function of frequency, ω, and for a fixed k.	39
6	Illustration of the phase speed as a function of along front wavenumber, γ.	44

Figure		Page
7	Illustration for what values of non-dimensional wavenumbers, λ and γ, that a wave would encounter a critical layer.	45
8	Contours of the fractional reflected energy in the λ-γ plane. The waves are incident from region I and the frontal shape defined by $\alpha_1 = .80$, $\alpha_2 = .16$, with $\beta^2 = 5$. $H_{11} > H_{12}$.	56
9	The fractional reflected energy as a function of angle of incidence for four values of non-dimensional frequency. Same parameters as listed in caption of figure 8.	58
10	The magnitude of incident, reflected and transmitted waves in polar co-ordinates. Each spoke in the incident and reflected wavefield indicates 15^{o}. The angle of the spokes in the transmitted part are listed in table 2. Three selected frequencies are shown. The frontal parameters are the same as those listed in the caption of figure 8.	61
11	Contours of the fractional reflected energy for waves incident upon a	

Figure		Page
11	front that is the mirror image of the one used to obtain figure 8. $H_{11} < H_{12}$.	63
12	Contours of the fractional reflected energy in the λ-γ plane, when $\alpha_1 = .80$, $\alpha_2 = .16$ and $\beta^2 = 1$. The pebbled region indicates the CLR. $H_{11} > H_{12}$.	73
13	Contours of the fractional transmitted energy in the λ-γ plane for the same parameters as listed in caption of figure 12. The pebbled region denotes the CLR.	74
14	The plot of the magnitudes of incident, reflected and transmitted waves in polar coordinates. The frontal parameters are the same as for figures 12 and 13.	76
15	Contours of the fractional reflected energy for waves that are incident upon a front that is the mirror image of the one discussed for figures 12-14.	79
16	Contours of the fractional transmitted energy associated with the fractional reflected energy in figure 15	80

Figure		Page
17	A plot of the magnitudes of the incident, reflected and transmitted waves in polar coordinates. The frontal parameters are the same as those for figures 15 and 16.	82
18	Contours of $\tilde{Q}(\lambda,\gamma)$. The positive value of the contours indicate that internal waves are gaining energy at the expense of the mean flow.	85
19	Schematic representation of the frontal profile in a three layer model.	87
20a	Using the parameters $\alpha_1 = \alpha_2 = .8$ $\alpha_3 = 0.$, $\alpha_4 = .11$, and $D = .6$, the frontal depth profile and the vertical modal structure are displayed.	107
20b	Fraction of energy reflected (R_1) and transmitted (T_1) in the same mode and the scattered reflected (R_2) and the scattered transmitted energy (T_2). The second mode is incident ($C_I=0$).	108
20c	Fraction of energy reflected (R_4) and transmitted (T_4) in the same mode, and the scattered reflected	

Figure		Page
20c	energy (R_3) and the scattered transmitted energy (T_3). The first mode is incident (A_I=0).	108
21a	Using the parameters α_1 = .8, α_2 = 0., α_3 = .13, α_4 = .11, and D = .5, the frontal depth profile and the vertical modal structure are displayed.	111
21b	The labels on the plots are the same as defined in 20b.	112
21c	The labels on the plots are the same as defined in 20c.	112
22a	Using the same frontal depthe parameters (α_i) as in figure 21 and D = .2, the frontal depth profile and the vertical modal strucute are displayed.	113
22b	The labels on the plots are the same as defined in 20b.	114
22c	The labels on the plots are the same as defined in 20c.	114

LIST OF TABLES

Table		Page
1	List of the layer depths in regions I and II, and the Rossby radius in each region for the three frontal shapes used in chapter 2.	25
2	List of incident angles (θ) and the resulting refracted angle (θ') for front with scales and depths as defined in table 3.	60
3	Typical scales and dimensional parameters for the front used in section 3.5 (without critical layers) and the front in section 3.6 (with critical layers).	72

THE REFLECTION, TRANSMISSION AND SCATTERING OF INTERNAL WAVES AT OCEAN FRONTS

I INTRODUCTION

There is a wide range of theoretical studies of the reflection, transmission and scattering of waves at oceanic topographic features (LeBlonde and Mysak, 1978 present numerous examples). However, the interactions of internal waves with horizontal inhomogeneities of the fluid have been examined only to a very limited extent. In the theoretical treatment of waves, any strong horizontal variability in the fluid is taken to be perpendicular to the direction of propagation of the wave. Usually any lack of horizontal homogeneity in the direction of propagation is assumed to be slowly varying and hence solved by WKB techniques. Within the ocean, however, there are regions where there are rapid changes in the medium. The purpose of this paper is to investi-

gate several characteristics (reflection, transmission, scattering, and both the production and absorbtion) of internal gravity waves at oceanic fronts. The study is limited to those fronts which do not intersect the surface or bottom of the ocean.

The model used here consists of a fluid of two (chapters 2 and 3) or more (chapter 4) layers. The depths of the layers are constant, except in the frontal region where the interface (interfaces) tilts upwards or downwards to form a density front. Associated with the front is a geostrophic current with non-zero horizontal shear. For the appropriate parameters critical layers occur and hence the absorbtion or production of internal wave energy. The defining equations consist of the linearized shallow water equations.

Olbers (1981) investigated a similar problem for a continuously stratified ocean. He was mainly interested in the scattering of internal gravity waves between the vertical modes. His method of solution assumes an identical density gradient upon each side of the front and that $U/c << 1$, where U is the mean velocity and c the

the phase speed. This inequality does not permit the occurance of critical layers.

II THE TWO LAYER MODEL WITH NORMAL INCIDENCE

In this chapter the reflection and transmission of internal gravity waves at a front in a two-layer fluid are investigated. The waves are normally incident upon the front and the reflection properties for an arbitrarily shaped interface are investigated.

2.1 Formulation of Problem

Figure 1 illustrates a transect of a two-layer, stably stratified ocean of constant total depth H. A frontal zone of width L separates two semi-infinite regions, in each of which the upper layer depth is constant. Cartesian coordinates, x,y,z, are chosen so that x is along the front, y is across the front and z is vertically upwards. The bottom is at z = 0, and the surface at z = H. The origin of y is placed at the intersection of the front with region I and the shape of the frontal interface is assumed to be uniform in the x-direction. The along front, across front and vertical components of velocity are u,v,w, respectively. In the upper and lower layers, denoted by subscripts i = 1 and i = 2, respectively, the densities ρ_i are constant. A rigid lid is imposed at the surface and the interface displacement is denoted by $\eta(x,y,t)$.

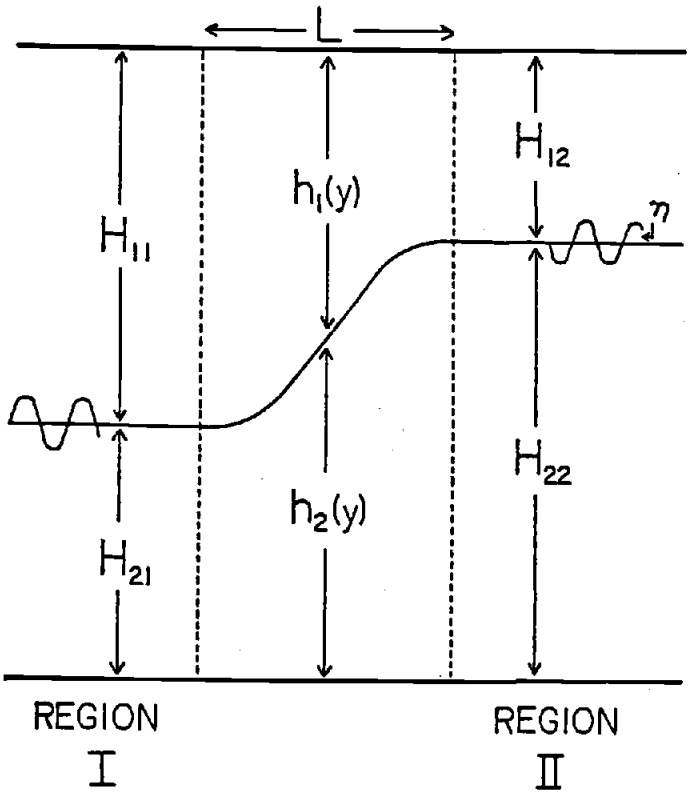

Figure 1: Schematic representation of the frontal profile.

For normal incidence the model has no x-dependence. The inviscid, vertically integrated shallow water equations are

$$u_{it} + v_i u_{iy} - f v_i = 0 \quad , \quad \text{for } i = 1,2$$

$$v_{it} + v_i v_{iy} + f u_i = -\rho_i^{-1} p_{iy} \quad , \quad \text{for } i = 1,2$$

$$h_{it} + (h_i v_i)_y = 0 \quad , \quad \text{for } i = 1,2$$

The Coriolis parameter, f, is assumed to be constant. In each layer, the motion is hydrostatic, so that if g is the gravitational acceleration, the pressures in the two layers are

$$p_1 = p_s + \rho_1 g(H-z)$$

$$p_2 = p_s + \rho_1 gH + (\rho_2-\rho_1) g h_2(y) - \rho_2 gz$$

Here p_s is the pressure at the surface and

$$h_1(y,t) = \bar{h}_1(y) - \eta(y,t)$$

$$h_2(y,t) = \bar{h}_2(y) + \eta(y,t)$$

$$H = \bar{h}_1(y) + \bar{h}_2(y)$$

Overbars will be used to denote steady state quantities so that in the above, $\bar{h}_1(y)$ and $\bar{h}_2(y)$ are the undisturbed depths of the upper and lower layers. These layer depths are always greater than zero.

The pressure and velocity fields are decomposed into the mean and perturbation components. Writing

$$p_1 = \bar{p}_s + \rho_1 g(H-z) + \rho_1 p \qquad (2.1a)$$

$$p_2 = \bar{p}_s + \rho_1 g h_1(y) + \rho_2 g(h_2(y)-z) + \rho_1 p \qquad (2.1b)$$

then the mean velocity is

$$(\bar{u}_1, \bar{v}_1) = (-f^{-1}\bar{p}_{sy}, 0) \qquad (2.1c)$$

$$(\bar{u}_2, \bar{v}_2) = (-f^{-1}(\bar{p}_s + g'\bar{h}_2)_y, 0) \qquad (2.1d)$$

where $g' = g(\rho_2-\rho_1)/\rho_1$ is the reduced gravity.

Assuming that the time dependence is of the form $\exp(-i\omega t)$ the linearized perturbation equations are

$$-i\omega u_1 + (\bar{u}_{1y} - f)v_1 = 0 \qquad (2.2)$$

$$-i\omega v_1 + f u_1 = -p_y \qquad (2.3)$$

$$i\omega\eta + (\bar{h}_1 v_1)_y = 0 \qquad (2.4)$$

$$-i\omega u_2 + (\bar{u}_{2y} - f)v_2 = 0 \qquad (2.5)$$

$$-i\omega v_2 + f u_2 = -(p_y + g'\eta_y) \qquad (2.6)$$

$$-i\omega\eta + (\bar{h}_2 v_2)_y = 0 \qquad (2.7)$$

From (2.4) and (2.7)

$$\bar{h}_1 v_1 + \bar{h}_2 v_2 = C \quad , \text{ a constant} \qquad (2.8)$$

This equation applies throughout the domain of y. In region II where $\bar{h}_2$ is a constant, the remaining momentum equations lead to

$$-i\omega(Hp + g'H_2\eta) = (\omega^2 - f^2)Cy + \text{const.}$$

The boundedness of the perturbation quantities requires that $C = 0$. Thus, there is no net transport in the across front direction. Equations (2.2)-(2.8) can be combined to form a single second order differential equation

$$V_{yy} + \left[\frac{(\omega^2-f^2)H}{\bar{h}_1(y)\bar{h}_2(y)g'} + \frac{f}{g'}\left(\frac{\bar{u}_{2y}}{\bar{h}_2} + \frac{\bar{u}_{1y}}{\bar{h}_1}\right)\right]V = 0 \quad (2.9)$$

where

$$V = \bar{h}_1 v_1$$

is the transport in the surface layer in the y-direction.

Except in the frontal region the mean depths are constant for each layer. Thus, in regions I and II (2.9) can be written as

$$v_{1yy} + \frac{H(\omega^2-f^2)}{H_1H_2g'}v_1 = 0 \quad (2.10)$$

where the constants H_1 and H_2 are the depths of the upper and the lower layers, respectively. This equation allows plane wave solutions

$$v_1 = Ae^{i\ell y} + Be^{-i\ell y}$$

where ℓ is a wavenumber that satisfies the dispersion relationship

$$\ell^2 = \frac{(\omega^2-f^2)H}{H_1H_2g'} \tag{2.11}$$

Thus for frequencies above the inertial (2.10) permits internal gravity wave solutions.

Consider a wave normally incident upon the front from region I. The wave will be partially transmitted into region II, while the remainder of its energy is reflected. Thus in region I we write

$$v_1 = A_Ie^{i(\ell y-\omega t)} + B_Re^{-i(\ell y+\omega t)} \tag{2.12}$$

where A_I and B_R are the incident and reflected wave amplitudes, respectively. As the wave propagates through the frontal region it is refracted, that is its wavenumber changes while the frequency, ω, remains constant. If ℓ' is the wavenumber in region II, then assuming that no wave is incident on the front from this side we write

$$v_1 = A_Te^{i(\ell'(y-L)-\omega t)} \tag{2.13}$$

where A_T is the amplitude of the tranmitted wave.

Using these amplitudes, the reflection coefficient is defined as

$$R = \left| \frac{B_R}{A_I} \right|$$

and the transmission coefficient is

$$T = \left| \frac{A_T}{A_I} \right|$$

It is useful to non-dimensionalize y and the wavenumbers ℓ, ℓ' with the frontal width (L) and $\bar{h}_1$, $\bar{h}_2$ with the layer depths of region I (H_{11} and H_{21}), then

$$\bar{h}_i = H_{i1} h_i \qquad i = 1,2$$

$$\ell = \lambda / L$$

$$\ell' = \lambda' / L$$

$$\bar{u}_i = \left(\frac{g' H_{i1}}{fL} \right) u_i \qquad i = 1,2$$

The non-dimensional form of (2.9) is then

$$V_{yy} + \left\{ \frac{\lambda^2}{h_1(y) h_2(y)} + \left(\frac{u_{2y}}{h_2(y)} + \frac{u_{1y}}{h_1(y)} \right) \right\} V = 0 \qquad (2.14)$$

The dispersion relationships for the non-dimensional wavenumbers λ and λ' are written as

Region I:

$$\lambda^2 = \left(\frac{\omega^2}{f^2} - 1\right) \frac{L^2}{\delta_1^2}$$

Region II:

$$\lambda'^2 = \left(\frac{\omega^2}{f^2} - 1\right) \frac{L^2}{\delta_2^2}$$

Here

$$\delta_i = \left[\frac{g' H_{1i} H_{2i}}{H}\right]^{\frac{1}{2}} f^{-1} \qquad i = 1,2$$

is the internal Rossby radius of deformation.

The boundary conditions, or more appropriately the matching conditions at the edges of the front are determined in the following manner. The normal transport, V , and the interface displacement, η, are both continuous at $y = 0$ and at $y = 1$. From (2.4), V_y must also be continuous at these points. Using (2.12) and its derivative, the matching conditions at $y = 0$, ((2.15a) and (2.15b)) can be derived in a straight forward manner. Similarly, (2.13) and its derivative yield (2.16a) and (2.16b).

$y = 0$:

$$V_y - i\lambda V = -2i\lambda H_{11} B_R \qquad (2.15a)$$

$$V_y + i\lambda V = 2i\lambda H_{11} A_I \qquad (2.15b)$$

$y = 1$:

$$V_y - i\lambda' V = 0 \qquad (2.16a)$$

$$V_y + i\lambda' V = 2i\lambda' H_{12} A_T \qquad (2.16b)$$

Here

$$\alpha = \left[\frac{H_{11}H_{21}}{H_{12}H_{22}}\right]^{\frac{1}{2}} = \lambda'/\lambda$$

and H_{12} and H_{22} denote the depths in region II of the upper and lower layers respectively. This formulation of the matching conditions allows easier implementation in the numerical scheme.

These four matching conditions, together with the second order differential equation (2.14) determines the ratios B_R/A_I and A_T/A_I.

The requirement that the transport, V, and the interface displacement, η, be continuous in y places restrictions on the mean interface shape. The integration of (2.14) from $y = -\epsilon$ to $y = +\epsilon$ results, when the limit $\epsilon \to 0$ is taken, in the following jump condition at $y = 0$

$$[u_1(0)] + [u_2(0)] = 0 \qquad (2.17a)$$

where

$$[u_i(0)] = \lim_{\varepsilon \to 0}(u_i(\varepsilon) - u_i(-\varepsilon)) \qquad i = 1,2$$

Similarly at $y = 1$

$$\frac{[u_1(1)]}{h_1(1)} + \frac{[u_2(1)]}{h_2(1)} = 0 \qquad (2.17b)$$

and here

$$[u_i(1)] = \lim_{\varepsilon \to 0}(u_i(1+\varepsilon) - u_i(1-\varepsilon)) \qquad i = 1,2$$

The mean velocity in the lower layer is usually taken to be zero. If this is done, then $u_1(y)$ must be continuous at both $y = 0$ and $y = 1$. So from (2.1c,d) the shape of the interface is restricted to cases where h_1 and h_{1y} are everywhere continuous. Thus an interface with a constant slope is not acceptable.

2.2 Energy Equation

It is both useful and informative to derive a relationship between the reflection coefficient (R) and the transmission coefficient (T). The most obvious equation to give the desired result, is an energy equation. Such a relationship would require only the calculation of the reflected energy to completely describe the partition of the energy which is incident

upon the front. It would also demonstrate whether or not there is any net exchange of energy between the mean and the perturbation velocities.

Scalar products of the transport vectors with the linearized momentum equations for each layer leads to an energy relation. This, when combined with the continuity equations and (2.8) results in

$$\frac{\partial E}{\partial t} - \frac{\partial F^y}{\partial y} + \bar{h}_1 \bar{u}_{1y} u_1 v_1 = 0 \qquad (2.18)$$

where

$$E = \bar{h}_1 K_1 + \bar{h}_2 K_2 + \tfrac{1}{2} g' \tilde{\eta}^2$$

with $K_i = \tfrac{1}{2}(u_i^2 + v_i^2)$ for $i = 1,2$ and

$$F^y = g' \bar{h}_1 v_i \tilde{\eta}$$

Outside the frontal region $\bar{u}_{iy} = 0$, and (2.18) becomes the classical energy equation, where E is the energy density and F^y the energy flux in the y-direction.

Let the time dependence be of the form

$$(u_i, v_i, \tilde{\eta}) \rightarrow (u_i, v_i, \eta) e^{-i\omega t}$$

Then integrating (2.18) over one period and taking the real part, we obtain

$$\frac{\partial}{\partial y}\left[g' \bar{h}_1 \{v_1^*(y)\eta(y) + v_1(y)\eta^*(y)\}\right] = \bar{h}_1 \bar{u}_{1y} \{u_1(y)v_1^*(y) + u_1^*(y)v_1(y)\} \qquad (2.19)$$

where * denotes the complex conjugate.

It is clear from (2.2) that

$$u_1^* v_1 + u_1 v_1^* = 0$$

Thus, there is no net exchange of energy between the mean flow and the perturbation flow. Applying the above relationship to (2.19) and integrating the resulting equation across the front, from $y = 0^+$ to $y = L^-$, yields

$$H_{11}(v_1^* \eta + v_1 \eta^*)\Big|_{y=0^+} = H_{12}(v_1^* \eta + v_1 \eta^*)\Big|_{y=L^-}$$

It only need be noted that both η and v_1 are continuous across the edges of the front and that

$$\eta = -H_{11}\ell/\omega \ (A_I e^{i\ell y} - B_R e^{-i\ell y})$$

in region I and

$$\eta = -H_{12}\ell'/\omega \ (A_T e^{i\ell'(y-L)})$$

in region II, to give the final relationship

$$R^2 + \left(\frac{H_{12}^2 \lambda'}{H_{11}^2 \lambda}\right) T^2 = 1 \qquad (2.20)$$

This is an equation relating the energy flux in two regions (I and II). In section 2.4, the transmission and reflection characteristics of the front will be discussed in terms of the fractional reflected energy, R^2.

2.3 Solutions

In theory the reflection coefficient can be determined by calculating the two independent series solutions for (2.14) and determining R from these results. It is not, in general, practical to use this method on the computer due to the slow rate of convergence of these series. Instead a numerical solution to the differentical equation is employed based on the recipe proposed by Lindzen and Kuo (1969). The exact method of implementation is discussed in Appendix A.

Two perturbation solutions will also be sought, one for large and the other for small non-dimensional wavenumber. For large λ the WKBJ method is appropriate and permits a qualitative discussion of the solution. An asymptotic solution for small λ is also undertaken. A comparison of these results to the numerical solution is made in section 2.4.

It is assumed that the lower layer has no mean motion ($\bar{u}_2=0$). As stated previously, this then requires that both h_{1y} and h_{2y} be zero at y = 0 and y = 1. Equation (2.14) is rewritten as

$$V_{yy} + \left[\frac{\lambda^2}{h_1(y)h_2(y)} - \frac{h_{1yy}}{h_1(y)}\right]V = 0 \qquad (2.21)$$

For large wavenumber, the asymptotic WKBJ solution for (2.21) can be obtained (following Nayfeh, 1973, p. 315) by assuming an expansion of the form

$$V(y;\lambda) = \{ \sum_{n=0}^{\infty} F_n(y) \lambda^{-n} \} e^{i\lambda\psi(y)}$$

After substituting this series into (2.21) and equating coefficients of like powers of λ, the order λ^2 and λ equations are

$$\psi'^2(y) = \{h_1(y)h_2(y)\}^{-1} \tag{2.22}$$

and

$$F_0(y) = C\{\psi'(y)\}^{-\frac{1}{2}} \tag{2.23}$$

where the prime denotes differentiation in y and C is a constant. The order λ^{-i+1} (for i = 1,2,...) equation is

$$2\psi'(y)F_i'(y) + \psi''(y)F_i(y) = i\left[\frac{u_1'(y)}{h_1(y)}F_{i-1}(y) + F_{i-1}''(y)\right] \tag{2.24}$$

Let $\psi(y)$ denote the integral of the positive root of (2.22), then

$$V(y;\lambda) = \{ \sum_{n=0}^{\infty} A_n(y)\lambda^{-n} \} e^{i\lambda\psi(y)} + \{ \sum_{n=0}^{\infty} B_n(y)\lambda^{-n} \} e^{-i\lambda\psi(y)}$$

To implement the boundary conditions it is necessary to expand the amplitudes of both the reflected wave, B_R, and the transmitted wave, A_T, in powers of λ.

Let

$$B_R = \sum_{n=0}^{\infty} R_n \lambda^{-n} \quad ; \quad A_T = \sum_{n=0}^{\infty} T_n \lambda^{-n}$$

Substitution of these series expansions in the boundary or matching conditions, (2.15) and (2.16), to lowest order, yield

$$A_0(0) = H_{11} A_I \, e^{-i\lambda\psi(0)}$$

$$B_0(0) = H_{11} R_0 \, e^{i\lambda\psi(0)}$$

$$B_0(1) = 0$$

Utilizing these along with the differential equations we have

$$B_0(y) = 0$$

and

$$R_0 = 0$$

Thus the reflection coefficient, R, for large wavenumber is at most of order λ^{-1}.

At the next order A_1 and B_1 satisfy the same equations as F_1 and F_0 (equations (2.24) and (2.23) respectively). Since the slopes of $h_1(y)$ and $h_2(y)$ are both zero at $y = 0$ and $y = 1$, then $A_0'(0) = 0$ and $A_0'(1) = 0$. The order λ^0 boundary conditions are then

$$B_1(0) = H_{11} R_1 \, e^{i\lambda\psi(0)}$$

$$A_1(0) = 0 \quad ; \quad B_1(1) = 0$$

Application of the boundary conditions to the differential equations gives

$$B_1(y) = 0$$

and

$$R_1 = 0$$

A non-zero reflection coefficient enters at the next order. It is not, necessary to consider the differential equation for $A_2(y)$. $B_2(y)$ once again satisfies (2.23). The relevant order λ^{-1} boundary conditions are

$$A_1'(0)\, e^{i\lambda\psi(0)} - 2i\psi'(0)\, B_2(0)\, e^{-i\lambda\psi(0)} = -2iH_{11}R_2$$

$$A_1'(1)\, e^{i\lambda\psi(1)} - 2i\psi'(1)\, B_2(1)\, e^{-i\lambda\psi(1)} = 0$$

Provided that the second derivatives of $h_1(y)$ and $h_2(y)$ are not zero at $y = 0$ and $y = 1$, these equations combine to yield the following relationship for the reflection coefficient

$$R^2 = (4\lambda)^{-4} \{ f^2(0) + f^2(1) - 2f(1)f(0)\cos(\lambda\xi)\} + o(\lambda^{-5}) \qquad (2.25)$$

where

$$f(y) = h_2''(y)h_1(y) - 3h_1''(y)h_2(y)$$

and

$$\xi = 2\{\psi(1) - \psi(0)\}$$

An examination of this solution is undertaken in section 2.4.

To obtain the solution for small wavenumber, the dependent variable and the amplitude of the reflected wave are expanded as

$$V = v_0 + \lambda v_1 + \lambda^2 v_2 + \lambda^3 v_3 + \ldots \qquad (2.26)$$

$$B_R = R_0 + \lambda R_1 + \lambda^2 R_2 + \lambda^3 R_3 + \ldots \qquad (2.27)$$

Substitution of (2.26) into (2.21) and the collection of coefficients of like powers of λ gives a set of second order ordinary differential equations that can be solved analytically. The solutions for the first four differential equations are

$$v_0 = h_1(y)\{C_1 + C_2 Q(y)\} \qquad (2.28)$$

$$v_1 = h_1(y)\{C_3 + C_4 Q(y)\} \qquad (2.29)$$

$$v_2 = h_1(y)\{C_5 + C_6 Q(y) + C_1 L_1(y) + C_2 L_2(y)\}$$

$$v_3 = h_1(y)\{C_7 + C_8 Q(y) + C_3 L_1(y) + C_4 L_2(y)\}$$

where the C_i's are constants and

$$Q(y) = \int^y h_1^{-2}(\xi)\, d\xi$$

$$L_1(y) = \int^y Q(\xi)h_1(\xi)h_2^{-1}(\xi)\,d\xi - Q(y)\int^y h_1(\xi)h_2^{-1}(\xi)\,d\xi$$

$$L_2(y) = \int^y Q^2(\xi)h_1(\xi)h_2^{-1}(\xi)\,d\xi - Q(y)\int^y Q(\xi)h_1(\xi)h_2^{-1}(\xi)\,d\xi$$

Substitution of (2.26) and (2,27) into the boundary conditions (2.15) - (2.16) and the collection of like powers of λ leads, at lowest order, to

$$v_0' = 0 \quad , \quad \text{at } y = 0,1$$

This with (2.28) implies that $C_2 = 0$. To next order, the boundary conditions are

$$v_1' - iv_0 = -2iH_{11}R_0 \quad , \quad \text{at } y = 0$$

$$v_1' + iv_0 = 2iH_{11}A_I \quad , \quad \text{at } y = 0$$

$$v_1' - i\alpha v_0 = 0 \quad , \quad \text{at } y = 1$$

where, as previously defined, $\alpha = \lambda'/\lambda$. From these (2.28) gives

$$C_1 = H_{11}(A_I+R_0)$$

Then from the boundary conditions and (2.29) two relationships for C_4 result

$$C_4 = iH_{11}(A_I-R_0)$$

$$C_4h_1^{-1}(1) = i\alpha v_0(1) = i\alpha H_{11}h_1(1)(A_I+R_0)$$

from which

$$\frac{R_0}{A_I} = \frac{1-\alpha h_1^2(1)}{1+\alpha h_1^2(1)}$$

The higher order boundary conditions are

$$v_i' - iv_{i-1} = -2iH_{11}R_{i-1} \quad , \text{ at } y = 0$$

$$v_i' + iv_{i-1} = 0 \quad , \text{ at } y = 0$$

$$v_i' - i\alpha v_{i-1} = 0 \quad , \text{ at } y = 1$$

for $i = 2,3,\ldots$. Using these matching conditions R_1/A_I and R_2/A_I may be derived in an analogous manner. Thus, the fractional reflected energy for small wavenumber is

$$R = \left| \frac{R_0}{A_I} + \frac{R_1}{A_I} + \frac{R_2}{A_I} \right| + o(\lambda^3)$$

$$= \{1-\alpha h_1^2(1)\}^2\{1+\alpha h_1^2(1)\}^{-2}$$

$$+ 4h_1^2(1)\lambda^2\alpha\{1+\alpha h_1^2(1)\}^{-4}\left[\{\int_0^1 h_1(y)h_2^{-1}(y)dy\}^2 + \right.$$

$$+\alpha^2 h_1^4(1)\{\int_0^1 h_1^{-2}(y)dy\}^2 - 2\int_0^1\{h_1(y)h_2^{-1}(y)\int_0^y h_1^{-2}(\xi)d\xi\}dy$$

$$\left. - 2\alpha^2 h_1^4(1)\int_0^1\{h_1(y)h_2^{-1}(y)\int_y^1 h_1^{-2}(\xi)d\xi\}dy\right] + o(\lambda^3) \qquad (2.30)$$

Notice that no order λ term appears, since R_1/A_I is purely imaginary, while R_0/A_I is purely real.

Once $h_1(y)$ and $h_2(y)$ are chosen, each integral can be evaluated numerically and the reflected energy for

small wavenumber determined. In the next section the solution for small λ is discussed.

2.4 Discussion of Solutions

To compare the two pertubation results to the numerical solutions it is necessary to define $h_1(y)$ and $h_2(y)$ explicitly. The simplest functions where $h_1'(y) = 0$ and $h_2'(y) = 0$ at $y = 0$ and $y = 1$, while the second order derivatives are non-zero at these points, are third order polynomials. The depths of the layers in the frontal zone are defined to be

$$h_1(y) = 1 - 3\alpha_1 y^2 + 2\alpha_1 y^3 \qquad (2.31)$$

$$h_2(y) = 1 - 3\alpha_2 y^2 + 2\alpha_2 y^3 \qquad (2.32)$$

where

$$\alpha_i = (H_{i1} - H_{i2})/H_{i1} \qquad i = 1,2$$

Figure 3a illustrates the shape of the interface for three values of α_1 and α_2: (a) $\alpha_1 = .80, \alpha_2 = .16$; (b) $\alpha_1 = .50, \alpha_2 = .10$; and (c) $\alpha_1 = .20, \alpha_2 = .04$.

The calculation of the fractional reflected energy as a function of non-dimensional wavenumber requires only that two paparmeters, α_1 and α_2, be specified. These parameters are normalized measures of the change in the upper and lower layer depths

across the front. Specifically, as α_1 or α_2 become small (large) the depth change across the front also becomes small (large). Table 1 gives possible values of the layer depths in region I and region II for the three values of α_1 and α_2 chosen. Also displayed are the internal Rossby radius of deformation for these depths, in each region.

The comparison of the analytic pertubation solutions to the numerical solution for a particular geometry (α_1 = .80 and α_2 = .16) is shown in figure 2. Within the regions where the perturbation solutions are valid, they are in good agreement with the numerical result. The wavelike behaviour for high wavenumber that is expected from the WKB solution (2.25) is displayed in this semi-log plot.

Several results can be deduced about the proportion of reflected energy from the examination of the analytic perturbation solutions (2.25) and (2.30) without explicitly defining $h_1(y)$ and $h_2(y)$. If (2.30) (small wavenumber perturbation solution) is considered first, then as $\lambda \to 0$, two generalities are evident. First, regardless of the shape of the interface in the frontal region, the fractional reflected energy is zero if and only if $H_{11} = H_{12}$.

Table 1. List of the layer depths in regions I and II, and the Rossby radius in each region for the three frontal shapes used in chapter 2.

(a) $\alpha_1 = .80$ $\alpha_2 = .16$

	i = 1	i = 2
H_{1i}	500 m	100 m
H_{2i}	2500 m	2900 m
δ_i	20.4 km	9.8 km

(b) $\alpha_1 = .50$ $\alpha_2 = .10$

	i = 1	i = 2
H_{1i}	500 m	250m
H_{2i}	2500 m	2750 m
δ_i	20.4 km	15.1km

(c) $\alpha_1 = .20$ $\alpha_2 = .04$

	i = 1	i = 2
H_{1i}	500m	400 m
H_{2i}	2500 m	2600 m
δ_i	20.4 km	18.6km

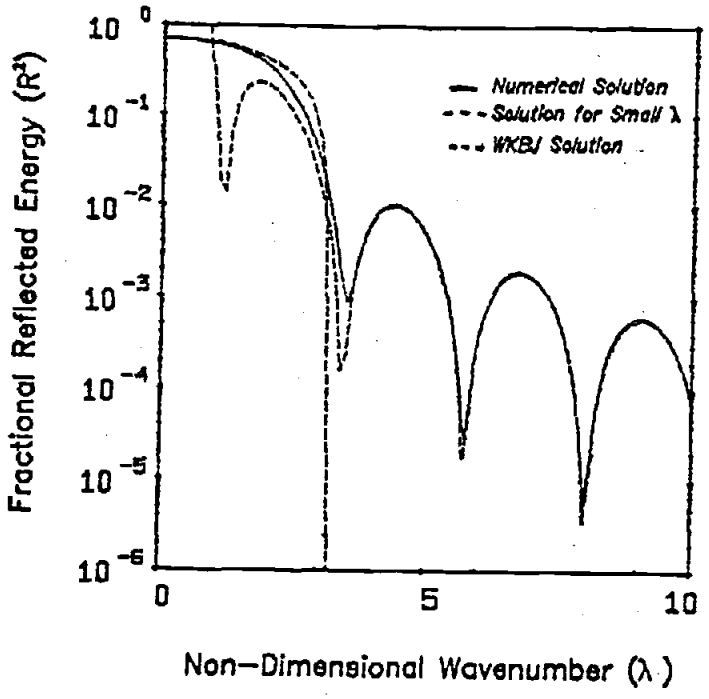

Figure 2: Comparison of the two perturbation solutions for α_1 = .80 and α_2 = .16.

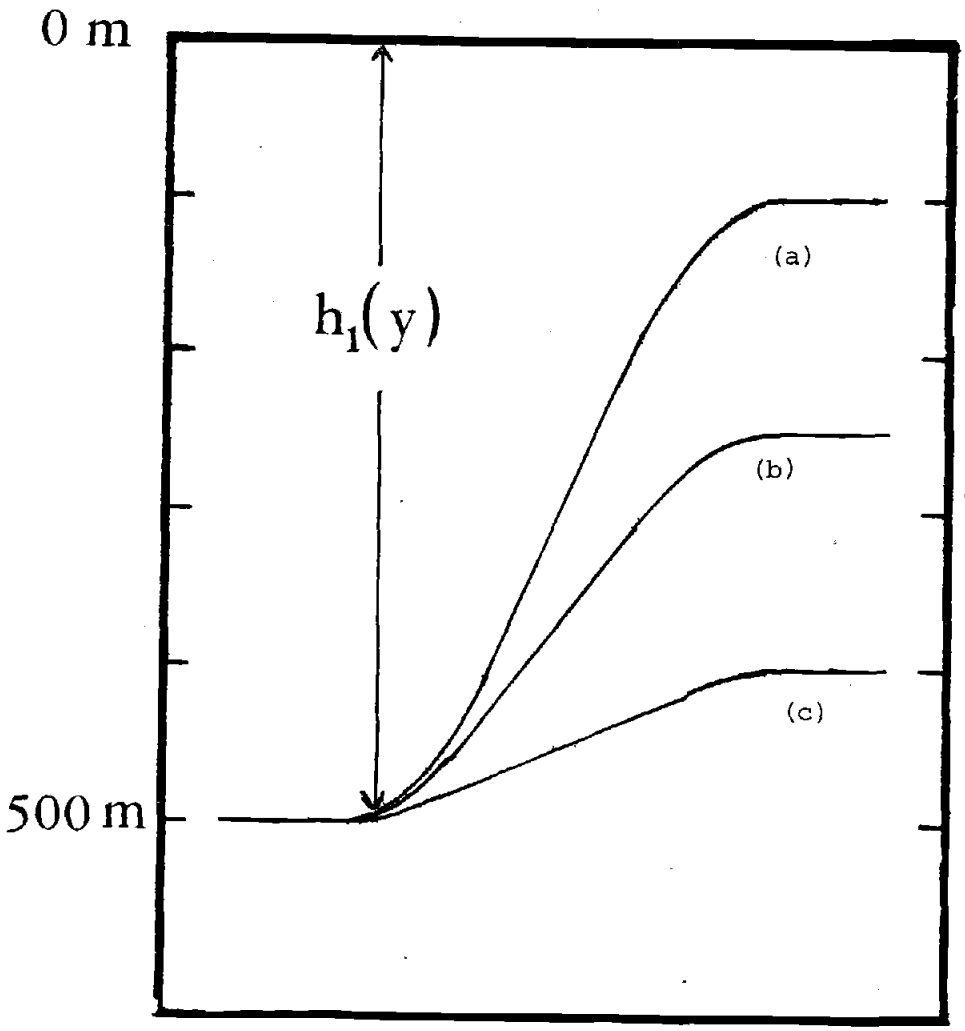

Figure 3a: Shape of the frontal interface for three values of α_1 and α_2: (a) $\alpha_1 = .80$, $\alpha_2 = .16$; (b) $\alpha_1 = .50$, $\alpha_2 = .10$; (c) $\alpha_1 = .20$, $\alpha_2 = .04$.

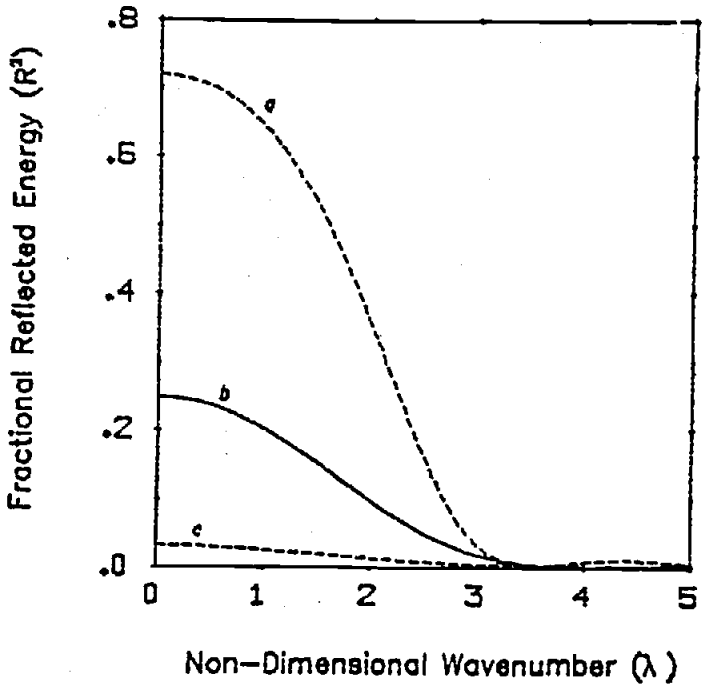

Figure 3b: The fractional reflected energy for the three profiles shown in figure 3a.

Second, the only way in which all the energy can be reflected is for the depth of the upper (or lower) layer to go to zero. The trend this implies is illustrated in figure 3b, where $h_1(y)$ and $h_2(y)$ are as defined in (2.31) and (2.32) and displayed in figure 3a. The wavenumber dependence of the fractional reflected energy is shown for the three values of α_1 and α_2 listed previously and given in table 1. As expected, as α_1 increase (the depth of the upper layer in ;region II approaches zero) the fractional reflected energy for small λ also increases.

At large wavenumbers, it is expected that the wave will be able to adjust to the variation in the layer depths and and for this reason little energy should be reflected. This is evident from (2.25) (WKB solution), where the fractional reflected energy decreases as λ^{-4}. It is assumed in the development of (2.25) that at $y = 0$ and $y = 1$, both h_{1y} and h_{2y} are zero. In general, from (2.24) and the matching conditions it can be concluded that R^2 decays as λ^{-2n} for large λ, when

i) $h_1(y)$ and $h_2(y)$ are both n-differentiable within the frontal region;

ii) the first (n-1) derivatives of $h_1(y)$ and $h_2(y)$ are zero at $y = 0$ and $y = 1$;

iii) the n^{th} derivative of $h_1(y)$ and $h_2(y)$ are zero at $y = 0$ and $y = 1$.

The examples shown in figure 3b are all drawn for cases where the upper layer depth of region I exceeds that of region II. With each example, an associated problem is that of the mirror image (about $y = \frac{1}{2}$) of the frontal profile. In the perturbation solutions, for small and large wavenumbers, the reflection coefficient, R_m for the mirror image problem can can be shown to be related to the original coefficient R through a rescaling of wavenumber

$$R_m^2(\lambda') = R^2(\lambda)$$

where

$$\lambda' = \left(\frac{H_{11}H_{21}}{H_{12}H_{22}}\right)^{\frac{1}{2}} \lambda$$

The numerical solution bears out the above result and also shows it to apply for intermediate wavenumbers.

The reflection of energy in the high wavenumber region is caused by different features of the front, than is the reflection for low wavenumbers. For high wavenumbers, the energy is reflected at discontinuities in the n^{th} derivatives of h_1 and h_2. The reflection for low wavenumbers, on the other hand, is caused by

differences at each side of the front in the wavelength and the depth of the layers. If these differences are too large, the long waves have insufficient space within the front in order to adjust. These waves are less affected than the short waves by discontinuities in the derivatives of the frontal profile.

In the real ocean, waves will be incident upon the front from both sides. To represent this situation we write

$$v_1 = \begin{cases} A_1 e^{i\lambda y} + B_1 e^{-i\lambda y} & , \text{ region I} \\ A_2 e^{-i\lambda'(y-1)} + B_2 e^{i\lambda'(y-1)} & , \text{ region II} \end{cases}$$

Here the A_i are the amplitudes of the incident waves and B_i combine the effects of transmission and reflection. For this situation of normal incidence the energy equation is

$$\left(|A_1|^2 - |B_1|^2 \right) = - \left(\frac{H_{12}^2 \lambda'}{H_{11}^2 \lambda} \right) \left(|A_2|^2 - |B_2|^2 \right)$$

If the wavefield is horizonatally symmetric (or isotropic) in one region then the above energy relationship implies that this must be the case in the other region, also. Note that in this restricted situation of normal incidence horizontally symmetric

means that the energy of the incoming wave equals that of the outgoing wave.

Figure 3b shows a rapid drop off in the reflected energy at high non-dimensional wavenumbers. In fact for $\lambda > \pi$ the reflected energy is below one percent for all three cases. This corresponds to dimensional wavelengths ($2\pi/\ell = 2\pi L/\lambda$) that are less than twice the frontal width. If the front is ten kilometers wide (for example) then there is no measurable effect of its presence on internal waves whose wavelength is less than twenty kilometers. For low wavenumbers where energy transmission through the front is limited, measurable effects are more likely. The frequency that corresponds to $\lambda = \pi$ and to a ten kilometer front for all three examples ((a), (b) and (c)) is $\omega = 6.5 \times 10^{-4}\ s^{-1}$.

III TWO LAYER MODEL WITH NON-NORMAL INCIDENCE

In this section the two layer model is extended to include the case in which waves are not necessarily incident perpendicular to the front. The situation is rendered more complex than that treated in chapter II through the occurance of critical layers in which energy exchange between the mean flow and the waves becomes possible.

3.1 The Model

The structure of the front and the coordinate frame employed in this chapter are as illustrated in figure 1. While non-normal incidence introduces an x-dependence in the perturbation fields, the frontal structure, the mean pressure gradient and the geostrophic velocities are considered as invariant in the along front direction. The beginning equations are once again the linearized shallow water equations for two layers.

$$u_{1t} + \bar{u}_1 u_{1x} + (\bar{u}_{1y} - f)\, v_1 = -p_x \tag{3.1}$$

$$v_{1t} + \bar{u}_1 v_{1x} + f\, u_1 = -p_y \tag{3.2}$$

$$-\eta_t - \bar{u}_1 \eta_x + (\bar{h}_1 u_1)_x + (\bar{h}_1 v_1)_y = 0 \tag{3.3}$$

$$u_{2t} + \bar{u}_2 u_{2x} + (\bar{u}_{2y} - f)\, v_2 = -(p + g'\eta)_x \tag{3.4}$$

$$v_{2t} + \bar{u}_2 v_{2x} + f u_2 = -(p + g'\eta)_y \qquad (3.5)$$

$$\eta_t + \bar{u}_2 \eta_x + (\bar{h}_2 u_2)_x + (\bar{h}_2 v_2)_y = 0 \qquad (3.6)$$

where $g' = g(\rho_2 - \rho_1)/\rho_2$ is the reduced gravity. The geostrophic velocity in the lower layer is taken to be zero ($\bar{u}_2(y) = 0$). As a result the steady state velocity in the upper layer is

$$\bar{u}(y) = \bar{u}_1(y) = -(g'/f)\,\bar{h}_{1y} \qquad (3.7)$$

The along front and the time dependence in the above equations are assigned the form of a travelling wave, $\exp(-i\omega t+ikx)$, where the frequency (ω) and the along front wavenumber (k) are both real. Equations (3.1) - (3.6) now become

$$i(k\bar{u} - \omega)u_1 + (\bar{u}_y - f)v_1 = -ikp \qquad (3.8)$$

$$i(k\bar{u} - \omega)v_1 + fu_1 = -p_y \qquad (3.9)$$

$$-i(k\bar{u} - \omega)\eta + ik\bar{h}_1 u_1 + (\bar{h}_1 v_1)_y = 0 \qquad (3.10)$$

$$-i\omega u_2 - fv_2 = -ik(p + g'\eta) \qquad (3.11)$$

$$-i\omega v_2 + fu_2 = -(p + g'\eta)_y \qquad (3.12)$$

$$-i\omega\eta + ik\bar{h}_2 u_2 + (\bar{h}_2 v_2)_y = 0 \qquad (3.13)$$

Outside the frontal region the constant mean depths of the upper and lower layers lead to solutions whose y-dependence takes the form $\exp(i\ell y)$. The fourth order

problem posed by (3.8) - (3.13) then leads to a dispersion equation for internal gravity waves where for selected ω and k, the across front wavenumber ℓ may have four distinct values, given by

$$(k^2 + \ell^2)\{(\omega^2-f^2)H - g'H_1H_2(k^2+\ell^2)\} = 0$$

Thus, either

$$\ell^2 = - k^2$$

leading to solutions in which the wave travels parallel to the front and its amplitude decays or grows exponentially with distance from the front, or

$$\omega^2 - f^2 = g'H_1H_2(k^2+\ell^2)/H \qquad (3.14)$$

In the above H_1 is the depth of the upper layer, H_2 that of the lower and H the total depth $(H_1 + H_2)$.

Outside the frontal region, the general solution for each perturbation variable take the form

$$A\, e^{i\ell y} + B\, e^{-i\ell y} + C\, e^{|k|y} + D\, e^{-|k|y}$$

Without loss of generality the across front wavenumber, ℓ, is taken to have the same sign as the frequency, ω, then A (B) represents the amplitude of waves travelling in the positive (negative) y-direction.

Initially consider the problem of waves incident upon the front from one side only, say region I of figure 1. The requirement that solutions be bounded

at infinity, is satisfied by

$$v_1 = \begin{cases} A_I e^{i\ell y} + B_R e^{-i\ell y} + De^{|k|y}, & y<0 \quad (3.15) \\ A_T e^{i\ell'(y-L)} + D'e^{-|k|(y-L)}, & y>L \quad (3.16) \end{cases}$$

Here A_I, B_R and A_T are the amplitudes of the incident, reflected and transmitted waves, respectively, with D and D' the amplitudes of the decaying components.

The geometry of the model is further illustrated in figure 4. In this figure, $h_1(y)$ is greatest at y = 0 and decreases toward y = L. The arrows indicate the directions of travel of the various wave components, which make angles θ, θ' with the normal to the front.

$$\theta = \tan^{-1}(k/\ell) \quad (3.17)$$

$$\theta' = \tan^{-1}(k/\ell') \quad (3.18)$$

Given k and ω the remaining two parameters of the problem, ℓ and ℓ', are determined by the dispersion relationship (3.14) and by the particular frontal geometry. The wavenumber normal to the front in region II is related to that in region I by

$$\ell'^2 = [H_{11}H_{21}(\ell^2+k^2)/(H_{12}H_{22})] - k^2 \quad (3.19)$$

where the H_{ij} are as depicted in figure 1. This can be written in the more familar form of Snell's Law

$$\sin\theta/\sin\theta' = \{H_{11}H_{21}/(H_{12}H_{22})\}^{\frac{1}{2}}$$

The wavenumber ℓ' is the same sign as ℓ. For a fixed non-zero k, the dependence of ℓ and ℓ' on ω are illustrated

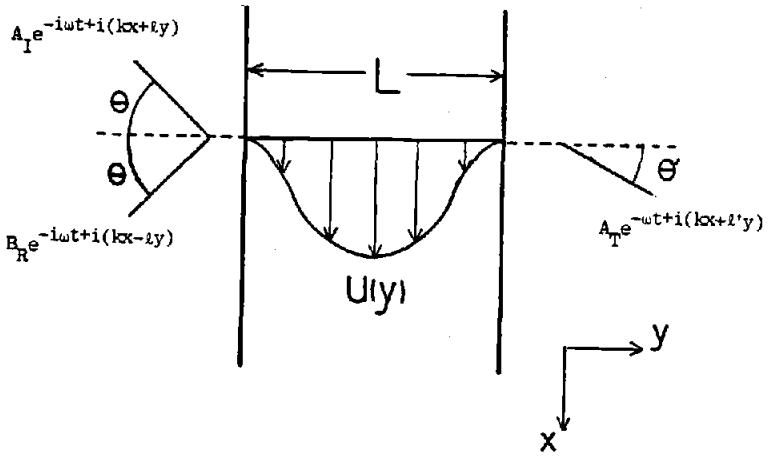

Figure 4: Schematic of the x-y plane, for waves that are not necessarily normally incident upon the front.

schematically in figure 5. Typically the upper layer depths (H_{11} and H_{12}) are much less than the lower layer depths (H_{21} and H_{22}). Figure 5a is the case where the upper layer depth is smaller in region I than in region II. In this situation, for each fixed non-zero k, a range of frequency (ω_1 - ω_2) exists for which the wavenumber ℓ' corresponding to ℓ, is purely imaginary, so that no travelling wave is possible in region II.

$$\omega_1^2 = f^2 + g'H_{11}H_{21}k^2/H$$

$$\omega_2^2 = f^2 + g'H_{12}H_{22}k^2/H$$

Alternately, when the upper layer depth in region I exceeds that in region II, there is always a real wavenumber ℓ' corresponding to ℓ as shown in figure 5b.

Figure 5 also illustrates the refraction that occurs when a wave passes through the front. When the upper layer depth is smaller in region I than in region II, the wave is refracted away from the normal ($\theta<\theta'$), while when the upper layer depth in region I exceeds that in region II the wave is refracted towards the normal ($\theta>\theta'$).

3.2 Matrix Representation

Equations (3.8) - (3.13) can be combined in a single fourth order or a pair of coupled second order

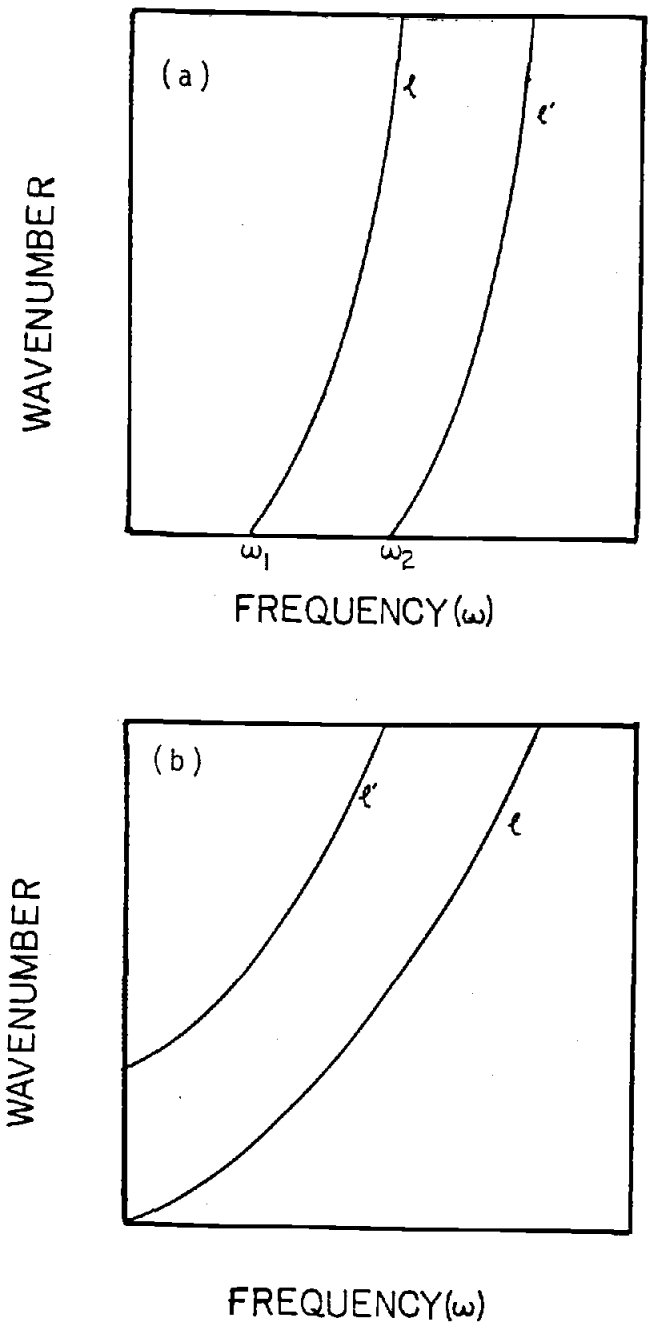

Figure 5: Sketch of the dispersion relationship for ℓ and ℓ' as a function of frequency, ω, and for a fixed k.

differential equations, but more insight into the mathematical properties of the system can be obtained if they are written as a set of first order differential equations.

$$(k\bar{u}-\omega)(\bar{h}_1 v_1)_y = k\bar{h}_1(\bar{u}_y-f)v_1 + ik^2 h_1 p + i(k\bar{u}-\omega)^2\eta$$

$$(k\bar{u}-\omega)p_y = -i\{(k\bar{u}-\omega)^2+f(\bar{u}_y-f)\}v_1 + kfp$$

$$\omega(k\bar{u}-\omega)\eta_y = i\omega\{(k\bar{u}-\omega)^2+f(\bar{u}_y-f)\}v_1 - fk^2\bar{u}p$$
$$- kf(k\bar{u}-\omega)g'\eta + i(k\bar{u}-\omega)(\omega^2-f^2)v_2$$

$$\omega(\bar{h}_2 v_2)_y = -ik^2\bar{h}_2 p + i(\omega^2-k^2\bar{h}_2 g')\eta + k\bar{h}_2 f v_2$$

The following scales are now introduced

$$(x,\ y,\ t,\ \omega) \rightarrow (L,\ L,\ f^{-1},\ f)$$

$$(v_i,\ p,\ \eta) \rightarrow (v_o,\ H_{11}g'v_o/fL,\ v_o fL/g')$$

for $i = 1,2$, where v_o is a value characteristic of the perturbation velocity. The steady state velocity and depths are scaled as

$$\bar{u} = g'H_{11}/(fL)\ u$$

$$\bar{h}_i = H_{i1}\ h_i \quad , \quad i = 1,2$$

and a non-dimensional transport is defined as

$$V_i = h_i v_i \quad , \quad i = 1,2$$

Non-dimensional wavenumbers in the across front direction (λ,λ') and the along front direction (γ) are defined through

$$\lambda = \ell L \; ; \; \lambda' = \ell' L \; ; \quad \gamma = kL$$

A matrix representation of the system of equations is

$$\underset{\sim}{\phi}_y = \frac{1}{\gamma_2(y)} \underset{\simeq}{A}(y) \; \underset{\sim}{\phi} \qquad (3.20)$$

where

$$\underset{\sim}{\phi}(y) = |V_1, \; p, \; \eta, \; V_2|^T$$

and

$$\underset{\simeq}{A}(y) = \begin{vmatrix} \gamma\gamma_4 & ih_1\gamma^2 & i\gamma_2^2 & 0 \\ -i\gamma_1/h_1 & \gamma\beta^2 & 0 & 0 \\ \dfrac{i\gamma_1}{\beta^2 h_1} & \dfrac{-\gamma^2 u}{\beta^2\omega} & \dfrac{-\gamma\gamma_2}{\omega} & \dfrac{i\gamma_2(\omega^2-1)}{\omega\, h_2} \\ 0 & \dfrac{-\gamma_2\gamma^2 h_2 i}{\beta^2\omega} & \dfrac{i\gamma_2\gamma_3}{\omega} & \dfrac{\gamma\gamma_2}{\omega} \end{vmatrix}$$

Here

$$\gamma_1 = \gamma_2^2 + \beta^2\gamma_4$$
$$\gamma_2 = \gamma u - \omega\beta^2$$
$$\gamma_3 = \beta^2\omega^2/q - h_2\gamma^2 \quad , \quad q = H_{21}/H_{11}$$
$$\gamma_4 = u_y - \beta^2$$

and β^2 is a non-dimensional number

$$\beta^2 = (Lf)^2/(g'H_{11})$$

In the domain D, $|y-\frac{1}{2}| < \frac{1}{2}$, the matrix $\underset{\approx}{A}(y)$ is analytic provided the front intersects neither the bottom nor the surface, and both $h_1(y)$ and $h_2(y)$ are analytic. When in this domain, $\gamma_2(y) \neq 0$, then the system has no singular points and the solutions are single valued. If, on the other hand there are points within D at which $\gamma_2(y) = 0$, then the domain in which $\underset{\approx}{A}(y)/\gamma_2(y)$ is analytic is no longer simply connected. At such points the solutions need not be single valued (Wasow, 1965).

The phase speed parallel to the mean flow is

$$c = \omega/\gamma$$

Thus if u_{max} is the maximum geostrophic velocity within the frontal region, from the definition of γ_2, the condition for single-valuedness is written

$$c > u_{max}/\beta^2$$

If for some y, $c = u(y)/\beta^2$, a critical point occurs.

Equation (3.14) in non-dimensional form is

$$\omega^2-1 = \frac{H_{21}}{\beta^2 H}(\gamma^2+\lambda^2)$$

For fixed λ, the phase speed as a function of γ that results is shown schematically in figure 6. As $\gamma \to \infty$, the phase speed decreases asymptotically to $(H_{21}/\beta^2 H)^{\frac{1}{2}}$.

If the condition for critical layers is satisfied the region in the λ-γ plane in which they occur is

$$\gamma^2 > \beta^2(\beta^2+H_{21}\lambda^2/H)(u_{max}^2 - \beta^2 H_{21}/H)^{-1}$$

as illustrated in figure 7. It should be noted that the sign of γ must be the same as that of u_{max}.

In obtaining solutions, the case of critical layers must be handled seperately from that in which no critical layers occur.

3.3 Matching Conditions

Across the edges of the front ($y = 0$ and $y = 1$), the normal velocities (v_1 and v_2), the pressure (p) and the interface displacement (η) are each taken to be continuous. As shown in section 2.1, the above condition on η requires that the geostrophic velocity, $u(y)$, be continuous. It simplifies the mathematics if it is further required that the geostrophic shear, u_y, be also continuous. In this study the depth of the upper layer in the frontal region is modelled with polynomial functions. The above additional requirement on u_y increases the order of the polynomial necessary,

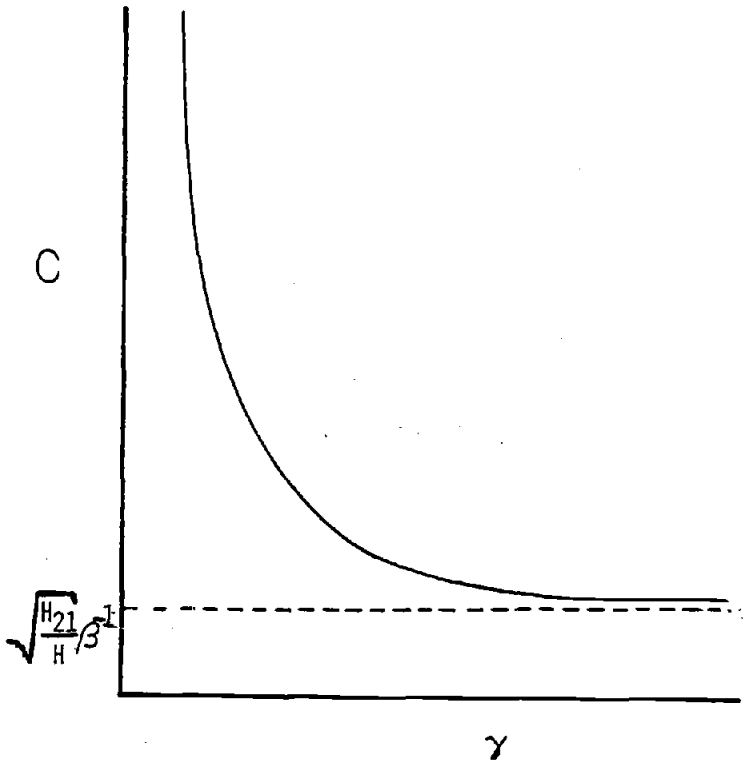

Figure 6: Illustration of the phase speed as a function of along front wavenumber, γ.

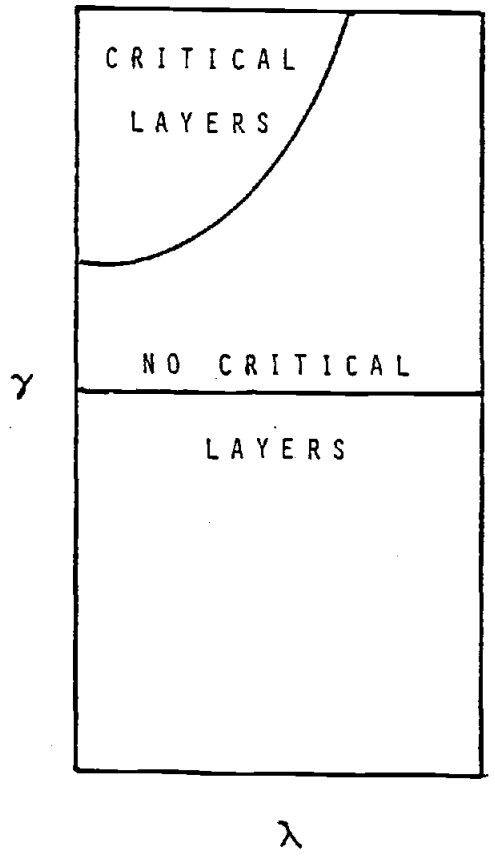

Figure 7: Illustration for what values of non-dimensional wavenumbers, and , that a wave would encounter a critical layer.

but does not alter energy reflection substantially. For large λ the amount of energy reflected will be proportional to λ^{-6} rather than to λ^{-4}. At small λ there is virtually no change.

Utilizing (3.15) and (3.16) in the matrix representation (3.20) the following relationships result.

Region I:

$$p = \beta^2(\omega^2-1)/(\gamma^2+\omega^2\lambda^2)\{(\omega\lambda+i\gamma)A_I e^{i\lambda y} - (\omega\lambda-i\gamma)B_R e^{-i\lambda y}\} + i\beta^2(\omega^2-1)/(\gamma+\omega|\gamma|)De^{|\gamma|y} \tag{3.21}$$

$$\eta = -\beta^{-2}(\lambda^2+\gamma^2)/(\gamma^2+\omega^2\lambda^2)\{(\omega\lambda+i\gamma)A_I e^{i\lambda y} - (\omega\lambda-i\gamma)B_R e^{-i\lambda y}\} \tag{3.22}$$

$$V_2 = -H_{11}(A_I e^{i\lambda y} + B_R e^{-i\lambda y})/H_{21} + De^{|\gamma|y} \tag{3.23}$$

Region II:

$$p = \beta^2(\omega^2-1)/(\gamma^2+\omega^2\lambda'^2)\{(\omega\lambda'+i\gamma)A_T e^{i\lambda'(y-1)}\} + i\beta^2(\omega^2-1)/(\gamma-\omega|\gamma|)D'e^{-|\gamma|(y-1)} \tag{3.24}$$

$$\eta = -H_{12}\beta^{-2}(\lambda'^2+\gamma^2)/\{(\gamma^2+\omega^2\lambda'^2)H_{11}\}\{(\omega\lambda'+i\gamma)A_T e^{i\lambda'(y-1)}\} \tag{3.25}$$

$$V_2 = -H_{12}(A_T e^{i\lambda'(y-1)})/H_{21} + H_{22}(D'e^{-|\gamma|(y-1)})/H_{21} \tag{3.26}$$

At $y = 0$ and $y = 1$, where V_1, p, η and V_2 are continuous, these relationships provide matching conditions.

3.4 Energy Equation

Again it is useful to derive a quantity that is invariant in the across front direction. An extension of the treatment used in section 2.2 leads to the energy relationship (in dimensional units)

$$\frac{\partial E}{\partial t} - \frac{\partial F^x}{\partial x} - \frac{\partial F^y}{\partial y} - + \bar{h}_1 \bar{u}_y u_1 v_1 - \bar{u} p \tilde{\eta}_x = 0 \qquad (3.27)$$

where

$$E = \bar{h}_1 K_1 + \bar{h}_2 K_2 + \tfrac{1}{2} g' \tilde{\eta}^2$$

with

$$K_i = \tfrac{1}{2}(u_i^2 + v_i^2) \qquad i = 1,2$$

and

$$F^x = -\{\bar{h}_1 \bar{u} K_1 + \bar{h}_1 u_1 p + \bar{h}_2 u_2 (p + g' \tilde{\eta})\}$$

$$F^y = -\{\bar{h}_1 v_1 p + \bar{h}_2 v_2 (p + g' \tilde{\eta})\}$$

Assuming a traveling wave dependence then

$$(v_i, u_i, p, \tilde{\eta}) = (v_i, u_i, p, \eta) e^{-i\omega t + ikx} \qquad i = 1,2$$

When (3.27) is integrated over one period $(2\pi/\omega)$ or one wavelength $(2\pi/k)$, we write

$$\frac{\partial}{\partial y}\left[\bar{h}_1 (v_1^* p + v_1 p^*) + \bar{h}_2 v_2^* (p + g' \eta) + \bar{h}_2 v_2 (p^* + g' \eta^*)\right]$$
$$+ \bar{h}_1 \bar{u}_y (u_1^* v_1 + u_1 v_1^*) - \bar{u} ik (p^* \eta - p \eta^*) = 0 \qquad (3.28)$$

Provided that $\gamma_2(y) \neq 0$, then using (3.8) - (3.10) (3.28) can be written in non-dimensional units as

$$\frac{\partial}{\partial y}\left[(1-u\gamma/\gamma_2)(V_1^*p+V_1p^*) + qV_2^*(p+\beta^2\eta) + qV_2(p^*+\beta^2\eta^*)\right] = 0 \quad (3.29)$$

The bracketed quantity is invariant in y. In the situation where $\gamma_2(y) = 0$ at some values of y, equation (3.29) still applies in the intervals between these critical points. Here only the case of no critical layers is considered and so (3.29) applies everywhere. (Critical layers are treated in section 3.6)

Equation (3.29) can be written in a different form by substituting (3.8) and (3.11) into it. Thus we have

$$\frac{\partial}{\partial y}\left[h_1(v_1^*u_1+v_1u_1^*) + qh_2(v_2^*u_2+v_2u_2^*))\right] = 0 \quad (3.29a)$$

The invariant quantity in (3.29a) is the total Reynolds stress (the sum of the Reynolds stress in the upper plus the lower layer which are weighted by the depths of each layer). This is a more useful quantity than (3.29), since it is easily measurable in the ocean.

Using the matching conditions of section 3.3, the invariant of (3.29) when evaluated at y = 0 and y = 1, leads to the relationships

$$\frac{H_{11}\lambda(\lambda^2+\gamma^2)}{\gamma^2+\omega^2\lambda^2}\{|A_I|^2-|B_R|^2\} = \frac{H_{12}\lambda'(\lambda'^2+\gamma^2)}{\gamma^2+\omega^2\lambda'^2}|A_T|^2 \quad (3.30)$$

for $H_{11}<H_{12}$ and all $\omega > 0$ (the case illustrated in figure 5b), and

$$|A_I|^2 - |B_R|^2 = 0 \qquad (3.31)$$

for $H_{11}<H_{12}$ and $\omega_1 < \omega < \omega_2$ (the case in figure 5a). Here ω_1 and ω_2 are as defined in section 3.1.

Once again it is only necessary to calculate the ratio of $|B_R|^2$ to $|A_I|^2$ to completely determine the transmission and reflection characteristics of a front without critical layers. For $\gamma = 0$, (3.30) reduces to the expression derived earlier for normal incidence.

3.5 Solutions Without Critical Layers

A general solution for the reflection and transmission properties of the frontal model requires a numerical treatment. Before obtaining such a solution it is instructive to examine perturbation solutions for certain limiting cases.

For small wavenumbers (γ,λ) define the linear relationship

$$\lambda = r\gamma$$

where r is an order one quantity. Each of the dependent variables of the model is expanded as a power series in γ. For example, let

$$V_1 = \sum_n V_{1n}\gamma^n$$

The amplitudes of the various wave components are similarly expanded.

$$B_R = \sum_n B_{Rn}\gamma^n \qquad A_T = \sum_n A_{Tn}\gamma^n$$

$$D = \sum_n D_n \gamma^n \qquad D' = \sum_n D'_n \gamma^n$$

For $\gamma = 0$, both D and D' are zero, thus the lowest order perturbation terms in their expansions, D_0 and D'_0, do not appear.

To lowest order the system of equations (3.20) yield

$$V_{10yy} = (h_{1yy}/h_1)\, V_{10}$$

This has solution

$$V_{10} = h_1(c_1 + c_2 \int^y h_1^{-2} d\xi)$$

Equations (3.8) and (3.10) combined with the requirement that the horizontal shear, u_y, be continuous for all y, imply that V_{1y} be continuous. The matching conditions are then

$$V_{10} = \begin{cases} A_I + B_{RO} & , \quad y = 0 \\ h_1 A_{TO} & , \quad y = 1 \end{cases}$$

$$V_{10y} = 0 \qquad , \quad y = 0,1$$

Thus, $V_{10} = c_1 h_1(y)$ where

$$c_1 = A_I + B_{RO} = A_{TO} \tag{3.32}$$

At the next order

$$V_{11y} - (h_{1yy}/h_1)V_{11} = c_1\beta^{-2}\{2h_{1y}h_{1yy} + h_1 h_{1yyy} - 2\beta^2 h_{1y}\}$$

which has solution

$$V_{11} = h_1(c_3 + c_4 \int^y h_1^{-2} d\xi) + c_1\beta^2 h_1 h_{1y} - 2c_1 h_1(\phi_1 + \phi_2 \int^y h_1^{-2} d\xi)$$

where

$$\phi_1(y) = -\int^y h_{1y} h_1 \int^\zeta h_1^{-2} d\xi d\zeta \quad ; \quad \phi_2(y) = \tfrac{1}{2} h_1^2$$

The relevant matching conditions for this solutions are

$$V_{11y} = \begin{cases} ir\,(A_I - B_{RO}) & , \quad y = 0 \\ ir\,\alpha\, h_1 A_{TO} & , \quad y = 1 \end{cases}$$

where again $\alpha = \lambda'/\lambda$. Thus

$$c_4 = h_1^2(1)(c_1 + ir\alpha A_{TO}) = c_1 + ir(A_I - B_{RO})$$

In combination with (3.32) this yields

$$\left|\frac{B_{RO}}{A_I}\right|^2 = \frac{\{1-h_1^2(1)\}^2 + r^2\{1-\alpha h_1^2(1)\}^2}{\{1-h_1^2(1)\}^2 + r^2\{1+\alpha h_1^2(1)\}^2}$$

This expression gives the limiting behavior as $\gamma \to 0$ ($\omega \to 1$) of the fractional reflected energy for r in the range, $0.5 < |r| < 5.0$. Since λ is always non-negative then r and γ must always be of the same sign. Notice that the fractional reflected energy is even in r for the limit $\gamma \to 0$. This is not surprising since in this limit ($\gamma \to 0$, $\omega \to 1$) the phase speed, c, tends to infinity, and the effect of the mean geostrophic velocity on the waves becomes negligible.

Now consider the small wavenumber perturbation solution when the incident wave almost parallels the front ($\lambda << \gamma << 1$). The first order differential equation and matching conditions for this situation are identical

to those of the lowest order expansions above. Thus equation (3.32) again applies. If $H_{11} > 2H_{12}$ then equation (3.19) implies that $\lambda << \lambda'$, and to lowest order the energy equation (3.30) yields

$$A_{T0} = 0$$

so that

$$R^2 = 1 \qquad , \qquad \lambda << \gamma << 1$$

Note that if $H_{11} < H_{12}$ (i.e. the upper layer depth increases in going from region I to region II), then (3.31) applies and $R^2 = 1$ results trivially.

The final small wavenumber solution to be considered here is that of almost normally incident waves, ($\gamma << \lambda << 1$). To lowest order the result (as expected from the analysis of section 2.3) is

$$R^2 = \left| \frac{1 - \alpha h_1^2(1)}{1 + \alpha h_1^2(1)} \right| \qquad , \quad \gamma << \lambda << 1$$

These three small wavenumber perturbation limits are discussed at greater length once the general numerical solution is obtained.

In obtaining a numerical solution, the recipe, adapted from Lindzen and Kuo, and used in the previous chapter is unsatisfactory. Higher resolution techniques are required, such as that mentioned in Acton (1970). This is implemented as described in Appendix C.

As in chapter 2, polynomials are used to represent the depths of the layers within the frontal zone. Fifth order polynomials are chosen whose first and second derivatives vanish at the edges of the front. As a result the geostrophic velocity and its horizontal shear are continuous throughout.

$$h_i(y) = 1 - \alpha_i y^3(10 - 15y + 6y^2) \quad , \quad i = 1,2$$

Here, as defined in chapter 2

$$\alpha_1 = (H_{11}-H_{12})/H_{11} \quad ; \quad \alpha_2 = (H_{21}-H_{22})/H_{21}$$

are used as normalized measures of the depth change across the front.

In this section solutions are discussed for the case of no critical layers. As shown in section 3.2 this requires that

$$\beta^2 = L^2 f^2/(H_{11} g') > H\, u_{max}^2/H_{21}$$

where u_{max} is the maximum geostrophic velocity. For the chosen frontal profile this occurs at $y = \frac{1}{2}$. Consider now a particular example where the relative depth change across the front is rather large: H_{11} = 500m, H_{12} = 100m, and with a total depth $H = H_{11}+H_{21}$ = 3000m. For these values u_{max} = 1.5 is the non-dimensional maximum geostrophic velocity, and to ensure no critical layers the condition $\beta^2 > 2.7$ must be satisfied. A

value of $\beta^2 = 5$ is chosen for the numerical example of this discussion. At mid latitudes ($f = 10^{-4}$ s^{-1}), with a reduced gravity $g' = 10^{-2}$ m s^{-2}, the corresponding frontal width, L, is 50 kilometers. For this example, $\bar{u}_{max} = 150$ cm s^{-1}. These values are listed in table 3 with the corresponding values for the case when there is a critical layer.

The results of the numerical calculation for this example are depicted in figure 8. Here the fractional reflected energy is contoured in the wavenumber (λ, γ) plane. Because of the energy relationship (3.30) a separate plot of fractional transmitted energy is not necessary. Certain general features are evident. For fixed γ, reflection decreases with increasing λ. The transmission is almost total in the lower right hand corner of the figure (λ large and γ negative). In contrast much of the energy is reflected in the upper right hand corner (λ large and γ positive). This lack of symmetry about the λ axis owes its origin to the presence of the geostrophic flow. For negative γ the wave travels in opposition to the geostrophic flow and so its relative velocity is more normal to the front, thus facilitating transmission. Conversely, for positive γ the relative velocity of the wave is more in alignment with the front and transmission is reduced.

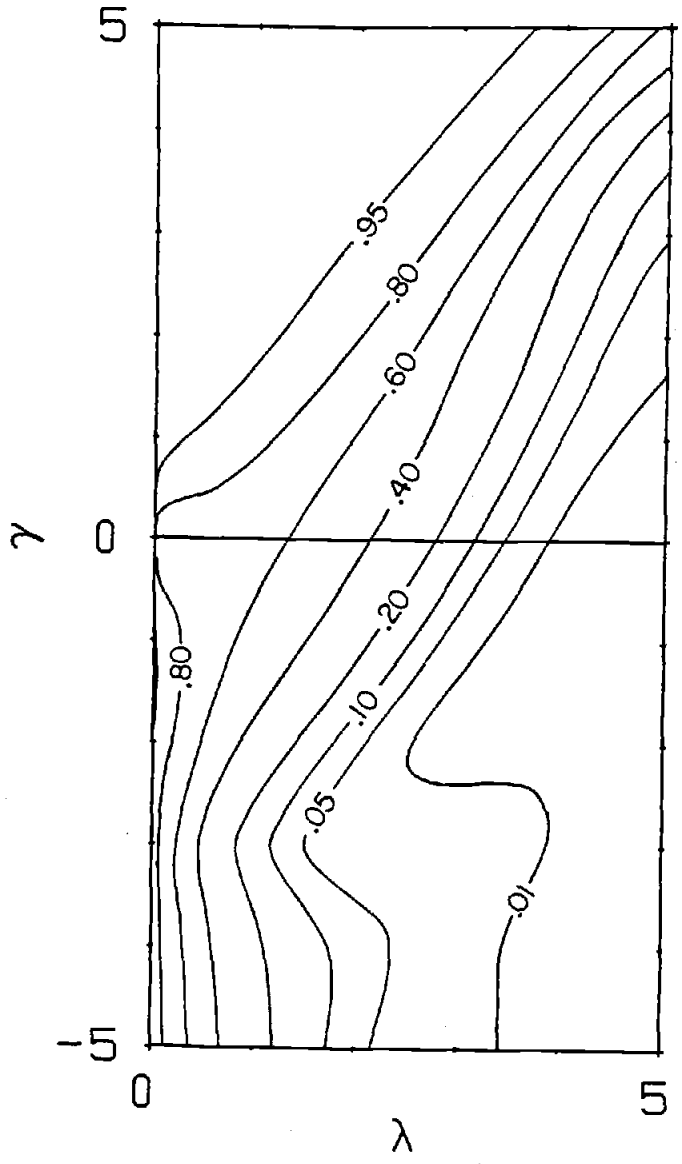

Figure 8: Contours of the fractional reflected energy in the λ-γ plane. The waves are incident from region I and the frontal shape defined by $\alpha_1 = .80$, $\alpha_2 = .16$, with $\beta^2 = 5$. $H_{11} > H_{12}$.

In the development of the model the hydrostatic approximation is made. For this to be valid then

$$\omega\left(\frac{H}{L}\right)^2 \ll 1$$

where the frequency, ω, is non-dimensional. Using the dispersion relationship and the appropriate dimensional quantities, we have

$$(\lambda^2+\gamma^2)^{\frac{1}{2}} \ll 680 \quad , \quad \text{Region I}$$

$$(\lambda'^2+\gamma^2)^{\frac{1}{2}} \ll 1400 \quad , \quad \text{Region II}$$

The contours displayed in figures 10 and 12 are well within these limits.

The contours of constant frequency in the λ-γ plane are semi-circles with centers at $\lambda=0$, $\gamma=0$. Figure 9 displays the fractional reflected energy along three of these curves as a function of incident angle. For a given frequency ($\omega > 1$) the reflection is almost total for large positive angles of incidence ($\theta > 50^{o}$). Maximum transmission is skewed towards negative angles of incidence. Also shown in this figure is the limiting case, $\omega \to 1$, derived from the three analytic perturbation solutions obtained at the beginning of this section. In this limit, the phase speed of the wave tends to infinity and the influence of the geostrophic flow becomes neglible. Hence the symmetric behavior is not surprising.

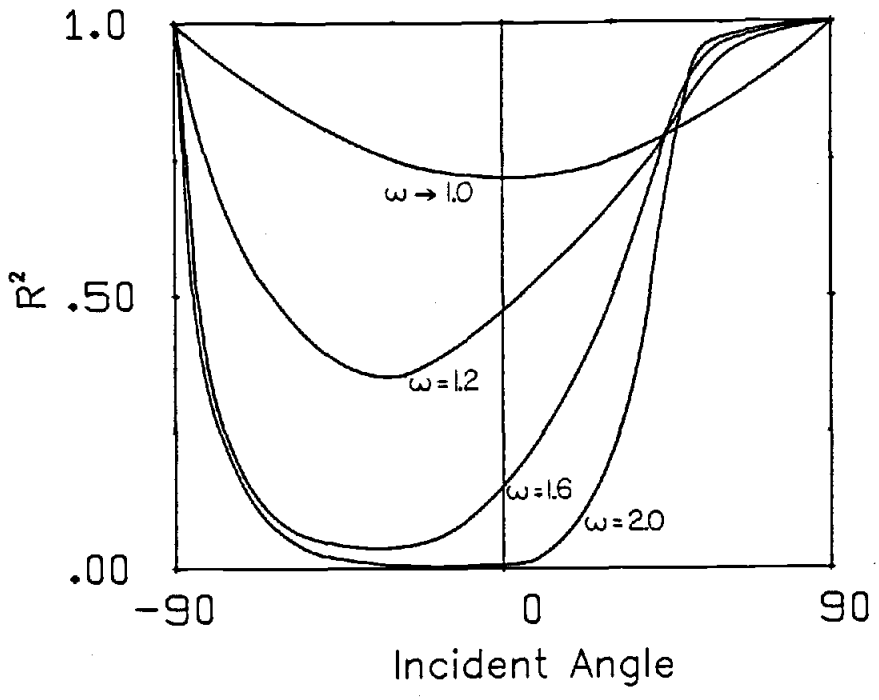

Figure 9: The fractional reflected energy as a function of angle of incidence for four values of the non-dimensional frequency. Same parameters as listed in caption of figure 8.

Consider the effect of the two layer frontal model on an isotropic wave field which is incident on the front from region I. Since the upper layer depth is assumed to be decreasing in going from region I to region II, the transmitted waves are refracted towards the normal. They emerge in a cone of semi-angle

$$\theta' = \sin^{-1}\left(\frac{H_{12}H_{22}}{H_{11}H_{21}}\right)^{\frac{1}{2}}$$

To illustrate this process, the dimensional and non-dimensional parameters listed in table 3 are used. In figure 10, for each of three distinct frequencies a polar representation of the amplitude of horizontally symmetric wavefield is displayed. Every 15^{o} is indicated. The resulting reflected wavefield is also displayed. A wave is reflected at the same angle at which it is incident, and so every 15^{o} is marked. The transmitted wavefield is also displayed. For the geometry used in this example the emergent cone has semi-angle, $\theta' = 28.8^{o}$. Each of the spokes in the incident wavefield is refracted toward the normal and their angle of imergence is noted in table 2. The maximum amplitude of the reflected component occurs at $\pm 90^{o}$ and has the same magnitude as that of the incoming wavefield. On the other hand, the maximum amplitude of the transmitted component varies with frequency and has been separately normalized in each case. The maximum transmission coefficient, T_m, and the angle of its occurance, θ'_m, are listed below for the three selected frequencies.

Table 2. List of incident angles (θ) and the resulting refracted angle (θ') for front with scales and depths as defined in table 3.

θ	θ'
$\pm 90^\circ$	$\pm 28.79^\circ$
$\pm 75^\circ$	$\pm 27.73^\circ$
$\pm 60^\circ$	$\pm 24.65^\circ$
$\pm 45^\circ$	$\pm 19.91^\circ$
$\pm 30^\circ$	$\pm 13.94^\circ$
$\pm 15^\circ$	$\pm 7.16^\circ$
$\pm 0^\circ$	$\pm 0^\circ$

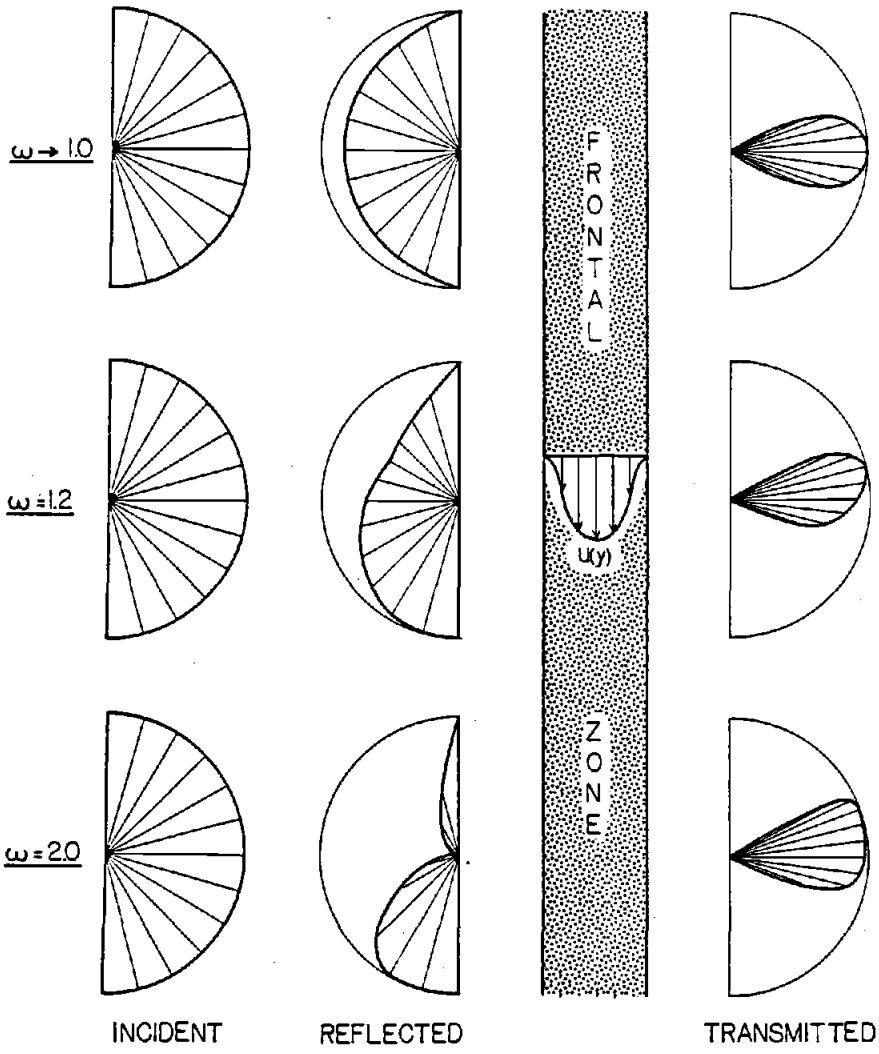

Figure 10: The magnitude of incident, reflected and transmitted waves in polar coordinates. Each spoke in the incident and reflected wavefield indicates 15^{o}. The angle of the spokes in the transmitted wavefield are listed in table 2. Three selected frequencies are shown. The frontal parameters are those listed in the caption of figure 8.

a) $\omega \to 1.0$, $T_m = 1.83$, $\theta'_m = 0^o$

b) $\omega = 1.2$, $T_m = 2.73$, $\theta'_m = -14^o$

c) $\omega = 2.0$, $T_m = 3.60$, $\theta'_m = -20^o$

As $\omega \to 1$ the reflection and transmission processes become symmetric, but with increasing frequency the reflected wavefield becomes increasingly asymmetric. The transmitted wavefield, confined as it is within a cone, is less distorted. In all cases, however, the process of reflection from and transmission through the front results in a highly non-isotropic wavefield.

If we now examine a front which is the mirror image (about $y = \frac{1}{2}$) of the example just discussed, a more complete understanding of the properties of the model is obtained. To maintain the non-dimensionalized geometry a value of $\beta'^2 = 25$ (corresponding to $\beta^2 = 5$ used above) is required. Now only waves incident on the front from region I, within a cone of semi-angle $\theta = 28.8^o$ may pass into region II. All waves outside this cone are totally reflected.

In figure 11 the fractional reflected energy is contoured for this situation. Areas of total reflection are evident and again an additional plot for transmitted energy is not required, because of equation (3.30). In fact, for this example in which there are

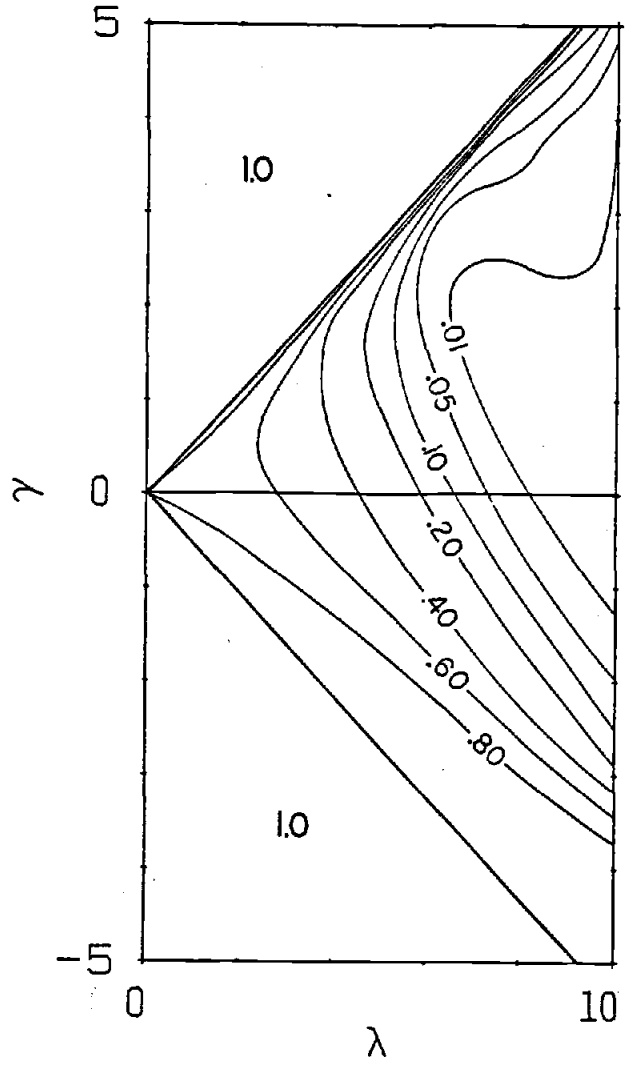

Figure 11: Contours of the fractional reflected energy for waves incident upon a front that is the mirror image of the one used to obtain figure 8. $H_{11} < H_{12}$.

no critical layers, if the across front wavenumber is transformed according to (3.19) and the along front wavenumber γ to $-\gamma$ then figure 8 and 11 are identical.

The situation when waves are incident upon both sides of the front is represented by

$$v_1 = \begin{cases} A_1 e^{i\lambda y} + B_1 e^{-i\lambda y} + D_1 e^{|\gamma| y} & \text{region I} \\ A_2 e^{-i\lambda'(y-1)} + B_2 e^{i\lambda'(y-1)} + D_2 e^{-|\gamma|(y-1)} & \text{region II} \end{cases}$$

The energy equation in this case is

$$\frac{H_{11}\lambda(\lambda^2+\gamma^2)}{\gamma^2+\omega^2\lambda'^2}\{|A_1|^2-|B_1|^2\} = \frac{H_{12}\lambda'(\lambda'^2+\gamma^2)}{\gamma^2+\lambda'^2\omega^2}\{|B_2|^2-|A_2|^2\}$$

If the wavefield is isotropic ($|A_i|^2=|B_i|^2$ for each λ and γ) in one region then it must also be isotropic in the other region.

3.6 Solutions with Critical Layers

If the same physical dimensions of the layer depths on each side of the front that are used in the previous section are once again considered, then for any $\beta^2<2.7$ (defined p. 42) a critical layer occurs. In fact, there are two critical points within the front. One is at $y = \frac{1}{2} + y_c$ and the other at $y = \frac{1}{2} - y_c$. There are two main methods of obtaining a solution when these critical points are considered. The first is to combine the system of equations (3.20) into one fourth order differential equation and obtain a Frobenius solution, as is done in LeBlond and Mysak (1978) for a second order differential equation. This method does not lend itself well to this fourth order system however. The alternate method is to introduce a small amount of linear damping (Jones, 1967), which then results in the frequency, ω, no longer being purely real. With this method, a numerical solution can be obtained by the same technique as used in previous section. The dimensional, linearized momentum equations with linear damping are

$$u_{1t} + \bar{u}u_{1x} + (\bar{u}_y - f)v_1 = -p_x - \tilde{r}u_1$$

$$v_{1t} + \bar{u}v_{1x} + fu_1 = -p_y - \tilde{r}v_1$$

$$u_{2t} - fv_2 = -(p+g'\eta)_x - \tilde{r}u_2$$

$$v_{2t} + fu_2 = -(p+g'\eta)_y - \tilde{r}v_2$$

where $\tilde{r}$ is a positive quantity and the continuity equations ((3.3) and (3.6)) remain unchanged. The $\tilde{r}u_i$ and $\tilde{r}v_i$ $(i = 1,2)$ are components of the frictional force or Rayleigh viscous force, in the x- and y-directions, respectively.

Once again let the time and the along front dependence be $\exp(-i\omega t+ikx)$. Here the wavenumber, k, is real (as before), but the frequency, ω, may be complex. The above equations along with (3.3) and (3.6) combine to form four first order, linear, coupled differential equations. When non-dimensionalized as in section 3.2, we have

$$\mu_2 V_{1y} = \mu_4 V_1 + i\gamma^2 h_1 p + i\mu_5\mu_2\eta \qquad (3.33)$$

$$\mu_2 p_y = -\mu_1 h_1^{-1} V_1 + \beta^2\gamma p \qquad (3.34)$$

$$\mu_2\omega'\eta_y = i\beta^{-2}\omega'\mu_1 h_1 V_1 - \gamma^2\beta^{-2}up - \gamma\mu_2\eta + i\mu_2(\omega'^2-1)h_2^{-1} V_2 \qquad (3.35)$$

$$\omega' V_{2y} = -i\gamma^2 h_2\beta^{-2}p + i\mu_3\eta + \gamma V_2 \qquad (3.36)$$

where

$$\omega' = \omega + ir$$

$$\mu_1 = \mu_2^2 + \mu_4\beta^2$$

$$\mu_2 = \gamma u - \beta^2\omega'$$

$$\mu_3 = \beta^2\omega\omega' q^{-1} - \gamma^2 h_2 \quad , \; q = H_{21}/H_{11}$$

$$\mu_4 = u_y - \beta^2$$

$$\mu_5 = \gamma u - \beta^2\omega$$

The frictional damping term, $\tilde{r}$, is non-dimensionalized with the Coriolis parameter, f. Since $\mu_2(y)$ is complex it is nonzero for all real y and a numerical solution can be obtained.

The dispersion relationship for this system of equations differs from (3.14). Letting the y-dependence be of the from $\exp(i\lambda y)$, then the non-dimensional dispersion relationship in region I is

$$(\gamma^2+\lambda^2)\left[(\omega'^2-1)\omega - \omega'(\lambda^2+\gamma^2)H_{21}/(H\beta^2)\right] = 0$$

and in region II

$$(\gamma^2+\lambda'^2)\left[(\omega'^2-1)\omega - \omega'(\lambda'^2+\gamma^2)H_{22}H_{12}/(HH_{11}\beta^2)\right] = 0$$

Denote the real part of the frequency as ω_r and the imaginary part as ω_i, then

$$(\omega_i+r)^3 - r(\omega_i+r)^2 + \tfrac{1}{4}(r^2+1+c)(\omega_i+r) - \tfrac{1}{8}rc = 0 \quad (3.37)$$

and

$$\omega_r^2 = 3(\omega_i+r)^2 - 2r(\omega_i+r) + 1 + c \quad (3.38)$$

where in region I

$$c = c_1 = (\lambda^2+\gamma^2)H_{21}/(H\beta^2)$$

and in region II

$$c = c_2 = (\lambda'^2+\gamma^2)H_{22}H_{12}/(HH_{11}\beta^2)$$

Since $c_1 = c_2$, (3.19) and Snell's law are still applicable.

It is evident from the perturbation solution to the cubic polynomial (3.37) that for small r there are a pair of complex conjugate roots and a real root to this cubic. Since both ω_r and ω_i are real, the solution of interest is, of course, the real root.

$$\omega_i = -r(1 + \tfrac{1}{2}c)/(1 + c) + o(r^3) \qquad (3.39)$$

Thus, the imaginary part of the frequency is less than or equal to zero and for sufficiently small r behaves in an almost linear manner in relation to r. Once ω_i is determined exactly, ω_r is easily calculated from (3.38). Using (3.39) we have

$$\omega_r = (1 + c)^{\frac{1}{2}} + o(r^2) \qquad (3.40)$$

which to lowest order is the dispersion relationship obtained when there is no linear damping. Note that the positive root of (3.38) is used , since once again the real part of the frequency is taken to be greater than zero.

The matching conditions are the same as those given in section 3.3, namely that V_1, V_2, p, and η are all continuous at y = 0 and y = 1. The relationships for V_2, p, η in regions I and II differ slightly, however.

Region I:

$$V_1 = A_I e^{i\lambda y} + B_R e^{-i\lambda y} + De^{|\gamma|y} \tag{3.41}$$

$$p = \beta^2(\omega'^2-1)\left[(\lambda\omega' - i\gamma)^{-1}A_I e^{i\lambda y} - (\lambda\omega' + i\gamma)^{-1}B_R e^{-i\lambda y} + (\gamma - i|\gamma|\omega')^{-1}De^{|\gamma|y}\right] \tag{3.42}$$

$$\eta = -\beta^{-2}(\lambda^2+\gamma^2)\frac{\omega'}{\omega}\left[(\lambda\omega' - i\gamma)^{-1}A_I e^{i\lambda y} - (\lambda\omega' + i\gamma)^{-1}B_R e^{-i\lambda y}\right] \tag{3.43}$$

$$V_2 = -(H_{11}/H_{21})(A_I e^{i\lambda y} + B_R e^{-i\lambda y}) + De^{|\gamma| y} \tag{3.44}$$

Region II:

$$V_1 = (H_{12}/H_{11})(A_T e^{i\lambda'(y-1)} + D'e^{-|\gamma|(y-1)}) \tag{3.45}$$

$$p = \beta^2(\omega'^2-1)\left[(\lambda'\omega'-i\gamma)^{-1}A_T e^{i\lambda'(y-1)} + (\gamma + i|\gamma|\omega')^{-1}D'e^{-|\gamma|(y-1)}\right] \tag{3.46}$$

$$\eta = -\beta^{-2}(H_{12}/H_{11})(\lambda'^2+\gamma^2)\frac{\omega'}{\omega}\left[(\lambda'\omega' - \gamma i)^{-1}A_T e^{i\lambda'(y-1)}\right] \tag{3.47}$$

$$V_2 = -(H_{12}/H_{21})A_T e^{i\lambda'(y-1)} + (H_{22}/H_{21})D'e^{-|\gamma|(y-1)} \tag{3.48}$$

Since at $y = 0$ and $y = 1$ V_1, p, η and V_2 are each continuous, these relationships provide the matching conditions at the edges of the front.

An energy relationship for this system can be obtained in the same manner that (3.27) is derived. Integration of this equation over one wavelength $(2\pi/\gamma)$ and over one period $(2\pi/\omega_r)$ yields a result similar to (3.28). If there is no critical layer, then as $r \to 0$, this equation collapses to (3.30). However, when $\mu_2 = 0$ for some y $(0 < y < 1)$ this is not true, and we write instead

$$\frac{H_{11}^2 \lambda(\lambda^2+\gamma^2)}{\gamma^2+\omega_r^2\lambda^2} \{|A_I|^2-|B_R|^2\} - \frac{H_{12}^2 \lambda'(\lambda'^2+\gamma^2)}{\gamma^2+\omega_r^2\lambda'^2} |A_T|^2 = Q(\gamma,\lambda)$$

When the numerical solution of the system (3.33) - (3.36) with its accompanying matching conditions is obtained, $Q(\gamma,\lambda)$ in the region where there are critical layers is not necessarily zero. A negative value indicates the production of internal wave energy at the expense of the mean flow and the front, and a positive value the absorption of internal wave energy.

Numerical solutions at selected points in the γ-λ plane are obtained for different vlaues of the frictional damping term ($r = 10^{-2}$, 10^{-3}, 10^{-4}, and 10^{-5}). There is virtually no variation in the resulting relative amplitudes (B_R/A_I, A_T/A_I, D/A_I, D'/A_I) between the solutions for the smaller three values of r and even the differences that occur between runs for $r = 10^{-2}$

and the others is less than half a percent. All the calculations shown in this section are accomplished with $r = 10^{-2}$.

Typical scales and dimensional parameters for a frontal model with critical layers are given in table 3. Also listed are the corresponding values for a front without critical layers that are used in obtaining the results of the last section. As can be seen, many of the parameters are identical. The choice of $\beta^2 = 1$ insures the occurance of a critical layer. (Recall, for the existence of critical layers the condition $\beta^2 < 2.7$ must be satisfied.) This smaller value of β^2 results in a narrower frontal width and in a stronger geostrophic current. For the hydrostatic approximation to be valid, $\omega H^2/L^2 \ll 1$ (ω is non-dimensional). That is, using the dispersion relationship,

$$(\lambda^2+\gamma^2)^{\frac{1}{2}} \ll 60$$

$$(\lambda'^2+\gamma^2)^{\frac{1}{2}} \ll 127$$

Figure 12 and 13 display the contours of the fractional reflected energy ($|B_R/A_I|^2$) and the fractional transmitted energy

$$\frac{H_{12}^2 \lambda'(\lambda'^2+\gamma^2)\quad(\gamma^2+\omega^2\lambda^2)}{H_{11}^2\,\lambda\,(\lambda^2+\gamma^2)\,(\gamma^2+\omega^2\lambda'^2)}\left|\frac{A_T}{A_I}\right|^2$$

respectively. Since there is no conserved property

Table 3. Typical scales and dimensional parameters for the front used in section 3.5 (without critical layers) and the front in section 3.6 (with critical layers).

	NO CRITICAL LAYERS	CRITICAL LAYERS
H_{11}(m)	500	
H_{12}(m)	100	
H_{21}(m)	2500	
H_{22}(m)	2900	
$f(s^{-1})$	10^{-4}	
$g'(m\ s^{-2})$	10^{-2}	
L(km)	50	22.4
β^2	5	1
$\bar{u}_{max}(cm\ s^{-1})$	150	223
$\left(\frac{H_{11}g'}{f^2}\right)^{\frac{1}{2}}$ (km)	22.4	
$\left(\frac{H_{12}g'}{f^2}\right)^{\frac{1}{2}}$ (km)	10.0	

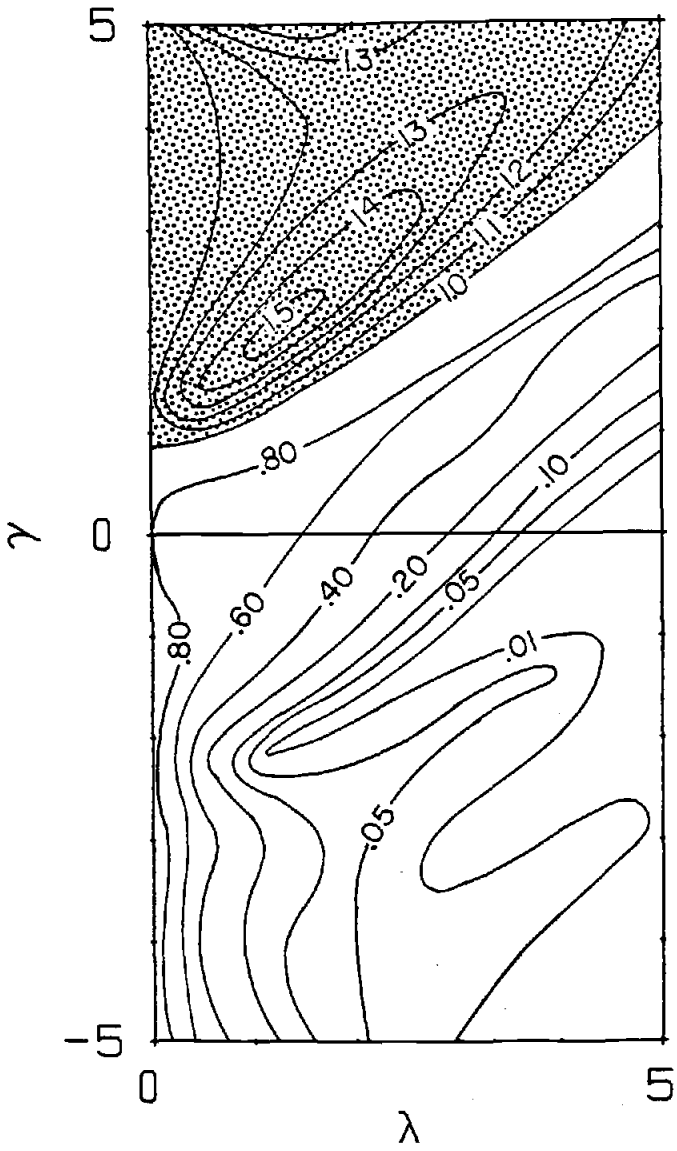

Figure 12: Contours of the fractional reflected energy in the λ-γ plane, when α_1 = .80 and α_2 = .16, with β^2= 1. The pebbled region indicates the CLR. $H_{11} > H_{12}$.

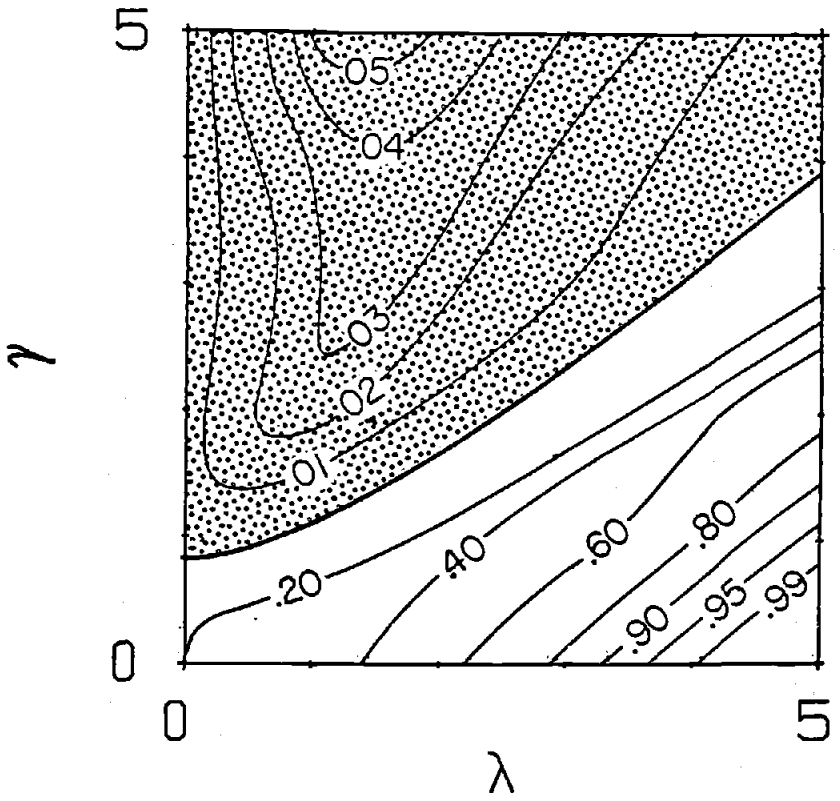

Figure 13: Contours of the fractional transmitted energy in the λ-γ plane for the same parameters as listed in caption of figure 12. The pebbled region denotes the CLR.

both of these quantities must be displayed. The pebbled region in both figures indicates the area in the λ-γ plane where critical layers occur (denoted by CLR in the following discussion). Outside this region there is a great similarity in the general features of figures 12 and 8, and the comments made in the previous section apply equally here. Within the shaded region over-reflection occurs. That is, there is more energy in the reflected wave than in the incident wave. This extra energy is gained from the mean flow. The greatest amount of over-reflection (in excess of 50% of the incident wave energy) occurs at $\gamma = 2$ and $\lambda = 1.5$. Notice that the majority of the energy gained from the mean flow is reflected and little is transmitted (figure 13). Outside of the CLR the energy relation (3.30) applies and it is not necessary to display the fractional transmitted energy explicitly.

Consider a horizontally symmetric wavefield, that is incident upon the front. In figure 14, for three distinct frequencies a polar representation of the amplitude of such an incident wavefield along with the reflected and transmitted amplitudes is displayed. Since the upper layer depth decreases in going from region I to region II, the transmitted waves are

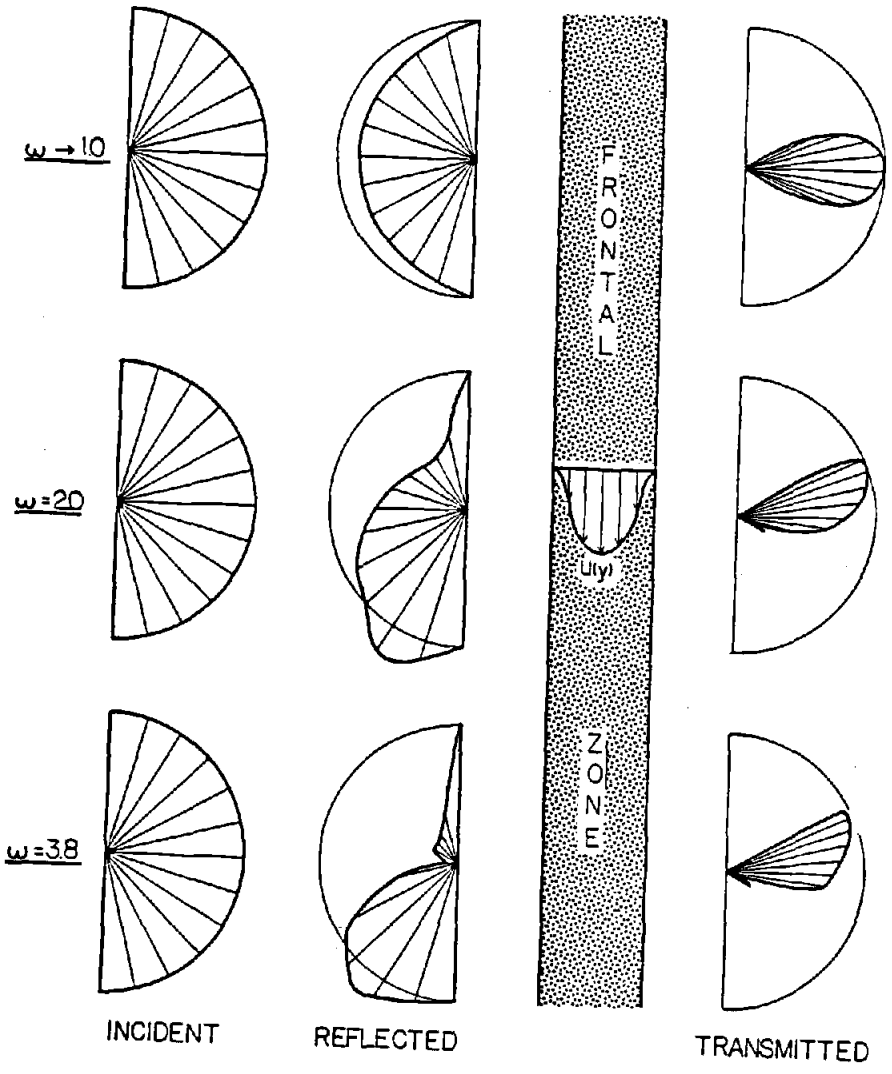

Figure 14: The plot of the magnitudes of the incident, reflected and transmitted waves in polar coordinates. The frontal parameters are the same as for figures 12 and 13.

refracted toward the normal and emerge in a cone of semi-angle, $\theta' = 28.8^{o}$. The contours of constant frequency in the λ-γ plane are semi-circles, with centers at $\gamma = 0$ and $\lambda = 0$. If the circle along which the frequency is constant does not intersect the CLR (in figure 14, $\omega \rightarrow 1.0$) then the maximum reflection occurs at $\theta = 90^{o}$, and has the magnitude of the incoming wave. On the other hand, if the semi-circle does intersect the CLR ($\omega = 2.0$ and $\omega = 3.8$, in figure 14), then the maximum reflection occurs away from $\theta = 90^{o}$. The transmitted amplitudes have been normalized with the maximum transmission coefficient for that frequency, T_m. The angle that this occurs at is θ_m. These are listed below for the three selected frequencies.

a) $\omega \rightarrow 1.0$, $T_m = 1.83$, $\theta'_m = 0^{o}$

b) $\omega = 2.0$, $T_m = 3.27$, $\theta'_m = 22^{o}$

c) $\omega = 3.8$, $T_m = 4.32$, $\theta'_m = 27^{o}$

The small lobe found in the transmitted amplitudes for $\omega = 2.0$ and $\omega = 3.8$ arises from the production of internal wave energy at the critical layers. The CLR also forces the transmitted wavefield to be more asymmetric than is found for the transmitted wave in figure 10.

Once again to gain a more complete understanding of the effect of a front upon internal wavefield, the

mirror image of the front just discussed is considered. To maintain the non-dimensionalized geometry a value of $\beta'^2 = 5$ (corresponding to $\beta^2 = 1$ used above) is required. As before only waves incident within a cone of semi-angle $\theta = 28.8^o$ can pass into region II. All waves outside this cone are totally reflected.

The contours of fractional reflected energy are displayed in figure 15 and of the fractional transmitted energy in figure 16. The behavior of the fractional reflected energy outside the CLR gives no new information since it is simply a transformation in wavenumber space ($\gamma,\lambda \rightarrow -\gamma,\lambda'$) of the contours from figure 12. Within the CLR this is not the situation. Not only is there over-reflection as in previous example, but also under-reflection - the absorbtion by the mean flow of energy in the internal wave field. The maximum over-reflection occurs at $\gamma \approx -2$ and $\lambda \simeq 2.5$, and amounts to 25% of the energy incident upon the front. The maximum under-reflection occurs at $\gamma \simeq -4$ and $\lambda' \approx 4$. Once again the energy that is gained from the mean flow is mainly reflected, with very little transmitted through the front (figure 16). The lower right hand part of the plot in figure 16 denotes the area of no transmission, since these waves are incident outside the cone of semi-angle 28.8^o.

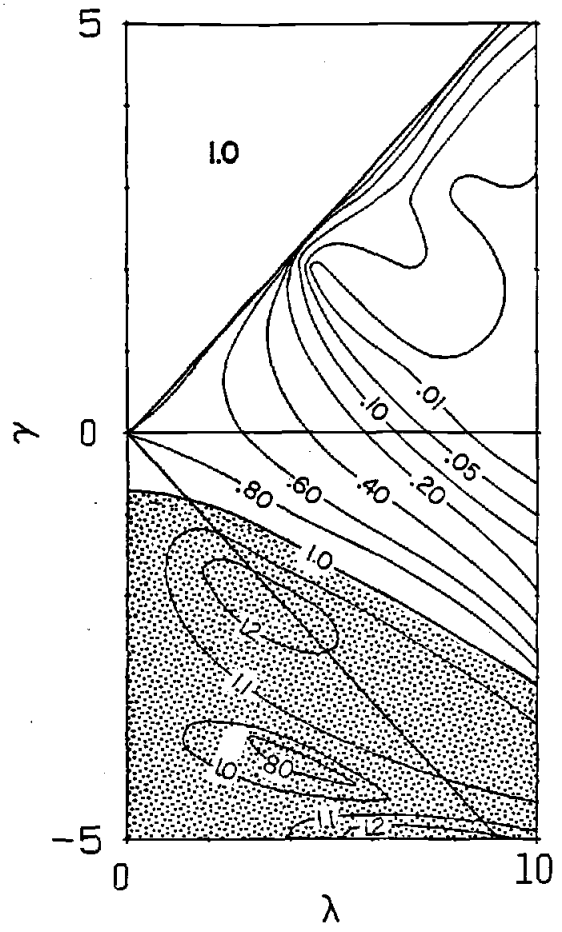

Figure 15: Contours of the fractional reflected energy for waves that are incident upon a front that is the mirror image of the one discussed for figures 12-14.

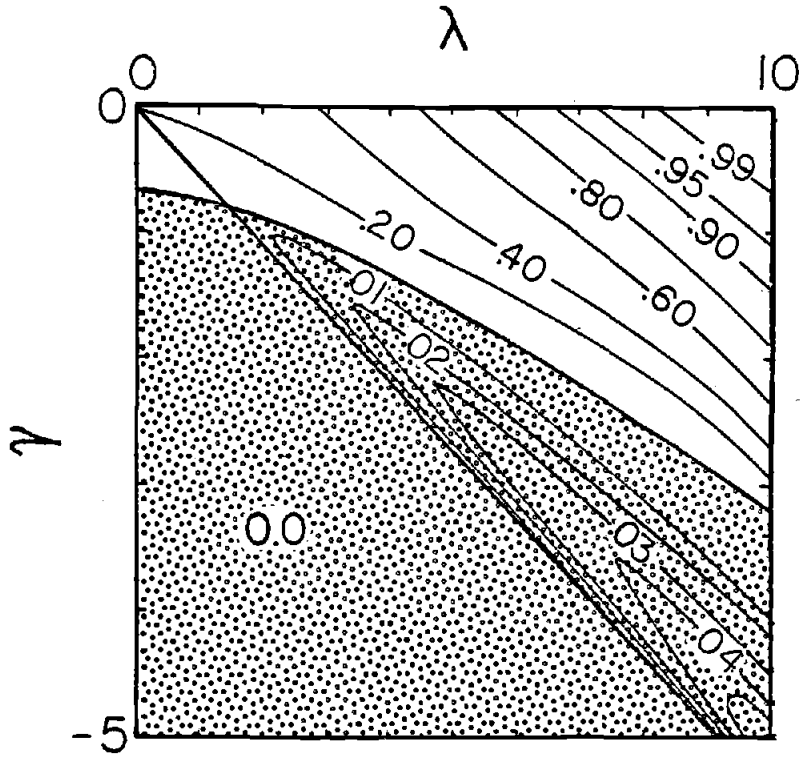

Figure 16: Contours of the fractional transmitted energy associated with the fractional reflected energy in figure 15.

The amplitudes of the isotropic incident wavefield and its accompanying reflected and transmitted wavefields are displayed in figure 17. The wave is assumed incident upon the front from region II and so we have the originally oriented front. The depth of the upper layer decreases from region I to region II. First consider a wave that is incident upon the front at an angle outside the cone of semi-angle 28^{o}. If these waves do not also pass through a critical layer they are totally reflected. If they do pass through one they are either over- or under-reflected. Any wave transmitted through the front is refracted away from the normal. Thus, the wavefronts would not appear to be parallel to the front. The amplitudes of the transmitted wave have, as before been normalized with the maximum amplitude, T_m. That, along with the angle the wave propagates at are listed below.

a) $\omega \rightarrow 1.0,\ T_m = .02,\ \theta_m' = 0^{o}$

b) $\omega = 2.0,\ T_m = .22,\ \theta_m' = 9^{o}$

c) $\omega = 3.8,\ T_m = .29,\ \theta_m' = 1^{o}$

The amplitudes of the transmitted waves are less than the amplitude of the incident wave on the other side of the front. The opposite is true when the waves are

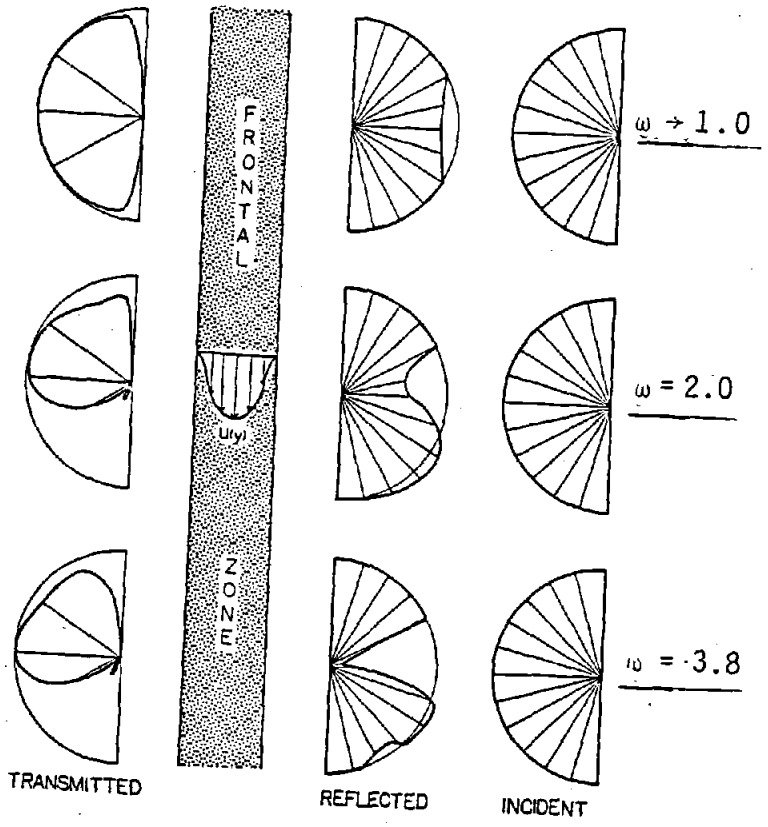

Figure 17: A plot of the magnitudes of the incident, reflected and transmitted waves in polar coordinates. The frontal parameters are the same as those for figures 15 and 16.

incident on the side of the front where the upper layer depths is deepest.

Consider now the situation where waves are incident upon both sides of the front simultaneously. That is

$$v_1 = \begin{cases} A_1 e^{i\lambda y} + B_1 e^{-i\lambda y} + D_1 e^{|\gamma| y} & \text{region I} \\ A_2 e^{-i\lambda'(y-1)} + B_2 e^{i\lambda'(y-1)} + D_2 e^{-|\gamma|(y-1)} & \text{region II} \end{cases}$$

The energy relationship is then written as

$$c_1\{|B_1|^2 - |A_1|^2\} + c_2\{|B_2|^2 - |A_2|^2\} = Q(\gamma,\lambda)$$

where

$$c_1 = \frac{H_{11}\lambda(\lambda^2+\gamma^2)}{\gamma^2+\omega_r^2\lambda^2}$$

$$c_2 = \frac{H_{12}\lambda'(\lambda'^2+\gamma^2)}{\gamma^2+\omega_r^2\lambda'^2}$$

Outside the CLR, as $r \to 0$ the $Q(\gamma,\lambda) \to 0$. Within the CLR it is a measure of how much energy is lost or gained by the wavefield. $Q(\gamma,\lambda)$ must be determined numerically. Consider the front already used in this section, namely that defined by the parameters in the second column of table 3. It is also necessary to

to define a relationship between the two incident amplitudes. Two choices immediately come to mind. The first is to let the amplitudes be equal and the second that the energies be equivalent. The second relationship is used here, namely $\sqrt{c}_1 \, |A_1| = \sqrt{c}_2 \, |A_2|$. Also only those waves whose cross front wavenumber in region I, λ, is greater that zero are considered. In figure 18 are displayed the contours of $\tilde{Q}(\lambda,\gamma) = Q(\lambda,\gamma)/\{\sqrt{c_1}|A_1|\}$ in the λ-γ plane. Note that $\tilde{Q}(\lambda,\gamma)$ is always positive for this particular frontal shape. That is the internal waves are gaining energy at the expense of the mean flow. Outside the CLR region (the pebbled area) $Q(\lambda,\gamma)$ is not exactly zero, since r is not zero, but is less than .02.

A comparison of the results of this section and the previous one to results obtained by Olbers (1981) is limited. The general comment that the greater the angle of incidence the greater the reflection and that the least amount of reflection is at near normal incidence, is a result of both analyses. The following section investigates in a small way the matter of scattering of wave energy from one vertical mode to another. Only waves that are normally incident are examined , however.

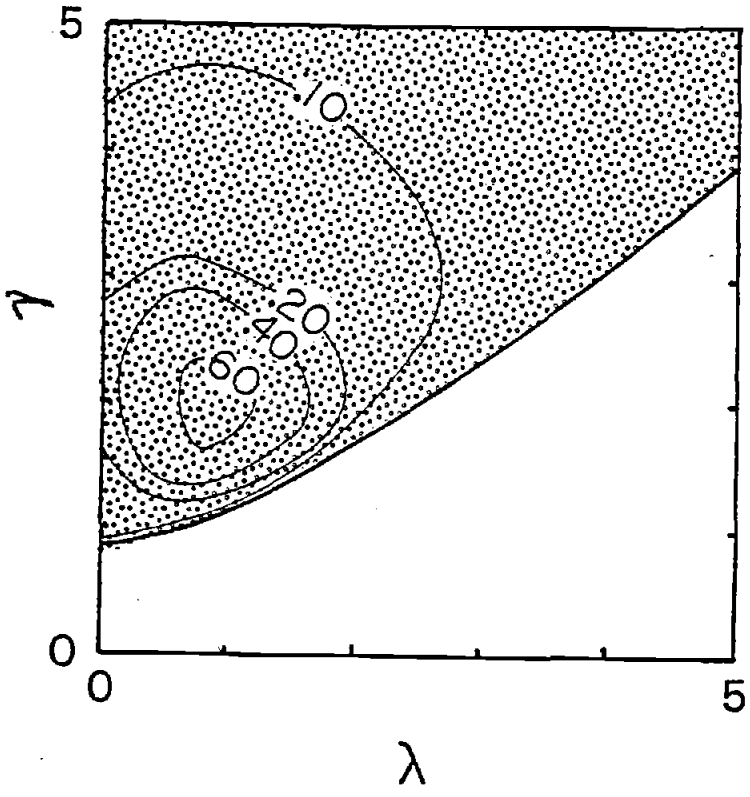

Figure 18: Contours of $\tilde{Q}(\lambda,\gamma)$. The positive value of the contors indicate that the internal waves are gaining energy at the expense of the mean flow.

IV THREE LAYER MODEL WITH NORMAL INCIDENCE

Although the two layer model with normally incident waves allows solutions that are easy to examine, the very simplicity of the model permits only reflection and transmission of the energy. In this chapter a model of three (or more) layers is investigated. Since such a model has more than one baroclinic mode, the energy of a wave incident upon the front in one vertical mode can be spread or scattered to the other baroclinc modes. The amount of energy scattered is, of course, depenedent upon the physical characteristics of the front.

A three layer model with waves that are normally incident allows a fourth order differential equation, or two coupled second order differential equations. The method in which the reflection and transmission coefficients are obtained is analogous to how they are obtained in the two layer model. Both a general numerical solution and WKB solution are obtained.

4.1 Formulation of the Problem

Figure 19 illustrates a transect of a three-layer stably stratified ocean of constant total depth H. If

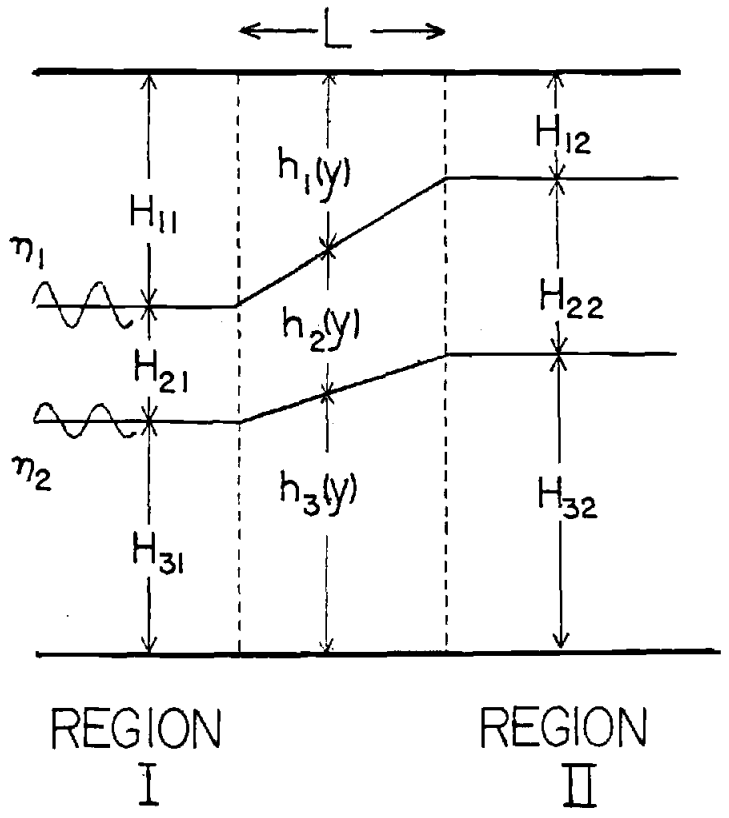

Figure 19: Schematic representation of the frontal profile in a three layer model.

the time dependence is of the form $\exp(-i\omega t)$, then the linearized, vertically integrated shallow water equations for three layers are

$$-i\omega u_1 + (u_{1y}-f)v_1 = 0 \tag{4.1}$$

$$-i\omega v_1 + fu_1 = -p_y \tag{4.2}$$

$$i\omega\eta_1 + (h_1 v_1)_y = 0 \tag{4.3}$$

$$-i\omega u_2 + (u_{2y}-f)v_2 = 0 \tag{4.4}$$

$$-i\omega v_2 + fu_2 = -p_y - g_1'\eta_{1y} \tag{4.5}$$

$$-i\omega\eta_1 + i\omega\eta_2 + (h_2 v_2)_y = 0 \tag{4.6}$$

$$-i\omega u_3 + (u_{3y}-f)v_2 = 0 \tag{4.7}$$

$$-i\omega v_3 + fu_3 = -(p_y + g_1'\eta_{1y} + g_2'\eta_{2y}) \tag{4.8}$$

$$-i\omega\eta_2 + (h_3 v_3)_y = 0 \tag{4.9}$$

where $\bar{u}_1$, $\bar{u}_2$ and $\bar{u}_3$ are the mean velocities and

$$g_1' = \frac{\delta_2 - \delta_1}{\delta_1} g \quad ; \quad g_2' = \frac{\delta_3 - \delta_2}{\delta_1} g$$

are the reduced gravities. If there is no mean motion in the lower layer ($\bar{u}_3 = 0$), then

$$\bar{u}_1 = -(g_1'\bar{h}_1 y + g_2'(\bar{h}_1+\bar{h}_2)_y)/f \tag{4.10}$$

$$\bar{u}_2 = -g_2'(\bar{h}_1+\bar{h}_2)_y/f \tag{4.11}$$

From (4.3), (4.6) and (4.9) we obtain a relationship for the net mass transport across the front

$$h_1 v_1 + h_2 v_2 + h_3 v_3 = C \quad , \text{ a constant} \qquad (4.12)$$

The manipulation of (4.1) - (4.9) results in the following relationship

$$-i\omega\{Hp+g_1'(H_{22}+H_{32})\eta_1 + H_{32}\eta_2\} = (\omega^2-f^2)Cy + \text{constant}$$

Thus, C = 0. That is the net transport is zero.

Equation (4.1) - (4.10) can be combined to form two coupled, second order differential equations in V_1 and V_2.

$$g_1' V_{1yy} + \bar{h}_1^{-1}(y)c_1 V_1 = \bar{h}_2^{-1}(y)c_2 V_2 \qquad (4.13)$$

$$g_1' g_2' \bar{h}_3 V_{2yy} + \bar{h}_2^{-1}\{(c_2\bar{h}_3+c_3 h_2)g_1' + c_2\bar{h}_3 g_2'\}V_2 = \bar{h}_1^{-1}\{c_1\bar{h}_3 g_2' - c_3\bar{h}_1 g_1'\}V_1 \qquad (4.14)$$

where

$$V_i = \bar{h}_i v_i \quad , \ i = 1,2$$

are the transports and

$$c_i = \omega^2 - f^2 + f\bar{u}_{iy} \ , \quad i = 1,2,3$$

Outside the frontal region the mean depth of each layer is constant and $\bar{u}_1 = 0$ and $\bar{u}_2 = 0$. Equation (4.13) and (4.14) can now be written as

$$H_1 g_1' v_{1yy} + (\omega^2-f^2)v_1 = (\omega^2-f^2)v_2 \qquad (4.15)$$

$$g_1' g_2' H_2 H_3 v_{2yy} + (\omega^2-f^2)\{(H_2+H_3)g_1' + H_3 g_2'\}v_2 = (\omega^2-f^2)(H_3 g_2' - H_1 g_1')v_1 \qquad (4.16)$$

where H_1 is the depth of the upper layer, H_2 the middle layer and H_3 the lower layer. Equations (4.15) and (4.16) are combined to form one fourth order differential equation in v_1 with constant coefficients.

$$v_1'''' + (\omega^2-f^2)(\gamma_{ai}^2+\gamma_{bi}^2)v_1'' + (\omega^2-f^2)\gamma_i^4 v_1 = 0$$

where

$$\gamma_{ai}^2 = \left[(H_{1i}+H_{2i})/(g_1' H_{1i} H_{2i})\right] (\omega^2-f^2)$$

$$\gamma_{bi}^2 = \left[(H_{2i}+H_{3i})/(g_2' H_{2i} H_{3i})\right] (\omega^2-f^2)$$

$$\gamma_i^4 = \left[H/(g_1' g_2' H_{1i} H_{2i} H_{3i})\right] (\omega^2-f^2)^2$$

Here i = 1 denotes region I and i = 2 region II. This equation allows plane wave solutions of the form $\exp(i\ell y)$. The dispersion relationship is

$$\ell = \left\{ \tfrac{1}{2}(\gamma_{ai}^2+\gamma_{bi}^2) \pm \tfrac{1}{2}\{(\gamma_{ai}^2+\gamma_{bi}^2)^2 - 4\gamma_i^4\}^{\frac{1}{2}} \right\}^{\frac{1}{2}} \qquad (4.17)$$

For frequencies above the inertial the plane wave solution to (4.15) and (4.16) are internal gravity waves.

There are two branches of the dispersion relationship. Initially consider the problem of waves incident upon one side of the front only, say region I in figure 19. Then we write

$$v_1 = \begin{cases} A_I e^{i\ell_1 y} + B_R e^{-i\ell_1 y} + C_I e^{i\ell_2 y} + D_R e^{-i\ell_2 y} & (4.18) \\ A_T e^{i\ell_1'(y-L)} + C_T e^{i\ell_2'(y-L)} & (4.19) \end{cases}$$

Here (4.18) is the behavior of v_1 in region I and (4.19) in region II. The wavenumbers ℓ_1 (ℓ_1') refers to the positive branch of the dispersion relationship and ℓ_2 (ℓ_2') to the negative branch in region I (region II).

When we investigate the proportion of the energy reflected and transmitted , either $A_I = 0$ or $C_I = 0$. If $C_I = 0$, then the reflection and transmission coefficients are

$$|B_R/A_I| \quad ; \quad |D_R/A_I| \quad ; \quad |A_T/A_I| \quad ; \quad |C_T/A_I| \tag{4.20}$$

Alternately, if $A_I = 0$, then they are

$$|B_R/C_I| \quad ; \quad |D_R/C_I| \quad ; \quad |A_T/C_I| \quad ; \quad |C_T/C_I| \tag{4.21}$$

These coefficients are used to define the fractional reflected and transmitted energies.

4.2 Modal Structure

Each branch of the dispersion relationship has associated with it a vertical modal velocity structure. Equation (4.15) and (4.16) are linear with constant coefficients and so there exists a similarity transfromation such that they can be rewritten in diagonal form

$$\phi_1'' + \mu_1^2\phi_1 = 0$$

$$\phi_2'' + \mu_2^2\phi_2 = 0$$

where ϕ_1 and ϕ_2 are linear combinations of v_1 and v_2, and μ_1 equals the positive branch of (4.17) and μ_2 the negative. The explicit relationship between v_1, v_2 and ϕ_1, ϕ_2 is

$$v_1 = \phi_1 + \phi_2$$

$$v_2 = \{1-H_1g'(\omega^2-f^2)^{-1}\mu_1^2\}\phi_1 + \{1-H_1g'(\omega^2-f^2)^{-1}\mu_2^2\}\phi_2$$

If we consider an incident wave of just one mode by letting $C_I = 0$ (i.e. $\phi_2 = 0$) then

$$v_1 = \phi_1$$

$$v_2 = \{H_2 - (H_1+H_2)\mu_1^2/\gamma_a^2\}H_2^{-1}\phi_1$$

$$v_3 = -(H_1+H_2)H_3^{-1}(1-\mu_1^2/\gamma_a^2)\phi_1$$

The other baroclinic mode ($A_I = 0$, $\phi_1 = 0$) has the vertical structure

$$v_1 = \phi_2$$

$$v_2 = H_2^{-1}\{H_2-(H_1+H_2)\mu_2^2/\gamma_a^2\}\phi_2$$

$$v_3 = -(H_1+H_2)H_3^{-1}(1-\mu_2^2/\gamma_a^2)\phi_2$$

In region I, the $H_j = H_{j1}$ and $\gamma_a^2 = \gamma_{a1}^2$ and in region II, $H_j = H_{j2}$ and $\gamma_a^2 = \gamma_{a2}^2$ for $j = 1,2,3$.

4.3 Non-dimensionalization

As in the previous chapters, y is non-dimensionalized with the across front width and the other parameters as follows

$$\ell_i = \lambda_i/L \quad ; \quad \ell_i' = \lambda_i'/L \qquad i = 1,2$$

$$\bar{h}_i = H_{i1} h_i \qquad i = 1,2,3$$

$$\bar{u}_i = H_{i1} g_1'/(fL)\, u_i \qquad i = 1,2$$

Equations (4.13) and (4.14) are now written in non-dimensional form as

$$V_{1yy} + \{f_{10}(y)\gamma^2 + f_{11}(y)\}V_1 = \{f_{12}(y)\gamma^2 + f_{13}(y)\}V_2 \qquad (4.22)$$

$$V_{2yy} + \{f_{20}(y)\gamma^2 + f_{21}(y)\}V_2 = \{f_{22}(y)\gamma^2 + f_{23}(y)\}V_1 \qquad (4.23)$$

where

$$f_{10}(y) = H_{21}\{(H_{11}+H_{21})h_1(y)\}^{-1}$$

$$f_{11}(y) = h_1^{-1}(y)u_1'(y)$$

$$f_{12}(y) = H_{11}\{(H_{11}+H_{21})h_2(y)\}^{-1}$$

$$f_{13}(y) = h_2^{-1}(y)u_2'(y)$$

$$f_{20}(y) = H_{11}(H_{11}+H_{21})^{-1}\{(H_{31}+H_{21})h_5(y)/(DH_{31}h_3(y))+1\}h_2^{-1}(y)$$

$$f_{21}(y) = (1+D^{-1})h_2^{-1}(y)u_2'(y)$$

$$f_{22}(y) = H_{21}(H_{11}+H_{21})^{-1}\{h_1^{-1}(y) - H_{11}/(DH_{31}h_3(y))\}$$

$$f_{23}(y) = f_{11}(y)$$

with $D = g_2'/g_1'$, $\gamma = \gamma_{a1}$ and $h_5 = (\bar{h}_2+\bar{h}_3)/(H_{21}+H_{31})$. The non-dimensional mean velocities are

$$u_1 = -(D+1)h_{1y}-D(H_{21}/H_{11})h_{2y}$$

$$u_2 = -D\{(H_{11}/H_{21})h_{1y}+h_{2y}\}$$

Examination of (4.22) and (4.23) shows that γ is related to the non-dimensional wavenumbers and so these equations are well suited to obtaining a WKB solution. Such a solution is obtained in section 4.6.

4.4 Boundary Conditions

The matching conditions at each edge of the front are the same as those employed in the two layer case, The normal transport in each layer (V_1, V_2 and V_3) are each continuous at $y = 0$ and $y = 1$ as are the interface displacements (η_1 and η_2). Examination of (4.3) and (4.6) shows that V_{1y} and V_{2y} are also continuous at the edges of the front.

For these to be useful it is necessary to know the explicit behavior of V_2, V_3, η_1 and η_2 in regions I and II. These are as follows.

Region I:

$$\eta_1 = -\omega^{-1}H_{11}\,\ell_1(A_I e^{i\ell_1 y}-B_R e^{-i\ell_1 y}) + \ell_2(C_I e^{i\ell_2 y}-D_R e^{-i\ell_2 y})$$

$$\eta_2 = -\omega^{-1}(H_{11}+H_{21})\Big[\ell_1(1-\ell_1^2/\gamma^2)(A\ e^{i\ell_1 y}-B\ e^{-i\ell_2 y}) + \ell_2(1-\ell^2/\gamma^2)(C\ e^{i\ell_2 y}-D\ e^{-i\ell_2 y})\Big]$$

$$v_3 = -H_{31}^{-1}(H_{11}+H_{21})\Big[(1-\ell_1^2/\gamma^2)(A_I e^{i\ell_1 y}+B_R e^{-i\ell_1 y}) + (1-\ell_2^2/\gamma^2)(C_I e^{i\ell_2 y}+D_R e^{-i\ell_2 y})\Big]$$

Region II:

$$\eta_1 = -\omega^{-1}H_{12}\Big[\ell_1' A_T e^{-i\ell_1'(y-L)} + C_T e^{-i\ell_2'(y-L)}\Big]$$

$$\eta_2 = -\omega^{-1}(H_{12}+H_{22})\Big[\ell_1'(1-\ell_1'^2/\gamma'^2)A_T e^{-i\ell_1'(y-L)} + \ell_2'(1-\ell_2'^2/\gamma'^2)C_T e^{-i\ell_2'(y-L)}\Big]$$

$$v_3 = H_{32}^{-1}(H_{12}+H_{22})\Big[(1-\ell_1'^2/\gamma'^2)A_T e^{-i\ell_1'(y-L)} + \ell_2'(1-\ell'^2/\gamma'^2)C_T e^{-i\ell_2'(y-L)}\Big]$$

where

$$\gamma'^2 = \gamma^2(H_{12}+H_{22})H_{21}H_{11}/\{H_{22}H_{12}(H_{11}+H_{21})\} = \gamma_{a2}^2$$

Integration of (4.13) and (4.14) about y = 0 and y = 1 (as is done in the two layer case), leads to the requirement that both $\bar{u}_1(y)$ and $\bar{u}_2(y)$ must be continuous at the edges of the front. This arises from the assumption that the interface heights be continuous at y=0 and 1.

4.5 Energy Equation

Following the treatment in section 2.2, leads to a quantity that is invariant in the across front direction. The application of the matching conditions to this quantity yields a relationship between the amplitudes.

If $C_I = 0$, then the relationship between the quantities listed in (4.20) is

$$1 = \left|\frac{B_R}{A_I}\right|^2 + \left(\frac{\lambda_2 D_2}{\lambda_1 D_1}\right)\left|\frac{D_R}{A_I}\right|^2 + \left(\frac{\lambda_1' D_3}{\lambda_1 D_1}\right)\left|\frac{A_T}{A_I}\right|^2 + \left(\frac{\lambda_2' D_4}{\lambda_1 D_1}\right)\left|\frac{C_T}{A_I}\right|^2 \qquad (4.24)$$

$$= R_1 + R_2 + T_1 + T_2$$

If, alternately, $A_I = 0$, then the relationship between the quantities listed in (4.21) is

$$1 = \left(\frac{\lambda_1 D_1}{\lambda_2 D_2}\right)\left|\frac{B_R}{C_I}\right|^2 + \left|\frac{D_R}{C_I}\right|^2 + \left(\frac{\lambda_1' D_3}{\lambda_2 D_2}\right)\left|\frac{A_T}{C_I}\right|^2 + \left(\frac{\lambda_2' D_4}{\lambda_2 D_2}\right)\left|\frac{C_T}{C_I}\right|^2 \qquad (4.25)$$

$$= R_3 + R_4 + T_3 + T_4$$

In both (4.24) and (4.25)

$$D_i = D(H_{11}+H_{21})^2(1-\lambda_i^2/\gamma^2)^2 + H_{11}^2 \qquad \text{for } i = 1,2$$

$$D_i = D(H_{12}+H_{22})^2(1-\lambda_i'^2/\gamma'^2)^2 + H_{12}^2 \qquad \text{for } i = 3,4$$

4.6 Solutions and Discussion

A general numerical solution is obtained in much the same manner as in the two layer case. The explicit details are given in Appendix A. As mentioned previously, the (4.22) and (4.23) are well suited to obtaining a WKB solution for high wavenumber. It is easiest to form one fourth order differential equation in V_1 to obtain such a solution. The resulting equation is

$$\begin{aligned}
&(g_{44}\gamma^4 + g_{42}\gamma^2 + g_{40})V_1'''' \\
&- 2(g_{34}\gamma^4 + g_{32}\gamma^2 + g_{30})V_1''' \\
&+ (g_{26}\gamma^6 + g_{24}\gamma^4 + g_{22}\gamma^2 + g_{20})V_1'' \\
&+ 2(g_{16}\gamma^6 + g_{14}\gamma^4 + g_{12}\gamma^2 + g_{10})V_1' \\
&+ (g_{08}\gamma^8 + g_{06}\gamma^6 + g_{04}\gamma^4 + g_{02}\gamma^2 + g_{00})V_1 = 0 \qquad (4.26)
\end{aligned}$$

where

$$g_{44} = f_{12}^2$$

$$g_{42} = 2f_{12}f_{13}$$

$$g_{40} = f_{13}^2$$

$$g_{34} = f_{12}f_{12}'$$

$$g_{32} = f_{12}f_{13}' + f_{12}'f_{13}$$

$$g_{30} = f_{13}f'_{13}$$

$$g_{26} = (f_{10}+f_{20})f_{12}^2$$

$$g_{24} = (f_{11}+f_{21})f_{12}^2 + 2(f_{10}+f_{20})f_{12}f_{13} + 2f_{12}^2 - f_{12}f''_{12}$$

$$g_{22} = (f_{10}+f_{20})f_{13}^2 + 2(f_{11}+f_{21})f_{12}f_{13} + 4f'_{12}f'_{13} - f_{12}f''_{13} - f_{13}f''_{12}$$

$$g_{20} = (f_{11}+f_{21})f_{13}^2 + 2f_{13}'^2 - f_{13}f''_{13}$$

$$g_{16} = f_{12}(f'_{10}f_{12} - f'_{12}f_{10})$$

$$g_{14} = f_{12}(f'_{11}f_{12} + 2f'_{10}f_{13} - f_{10}f'_{13}) - f'_{12}(f_{13}f_{10} + f_{11}f_{12})$$

$$g_{12} = f_{13}(2f_{12}f'_{11} + f_{13}f'_{10} - f_{10}f'_{13} - f_{11}f'_{12}) - f_{12}f_{11}f'_{13}$$

$$g_{10} = f_{13}(f'_{11}f_{13} - f_{11}f'_{13})$$

$$g_{08} = f_{12}^2(f_{10}f_{20} - f_{12}f_{22})$$

$$g_{06} = f_{12}^2(f''_{10} - f_{23}f_{12} - 3f_{13}f_{22} + f_{11}f_{20} + f_{21}f_{10}) + 2f_{12}'^2 f_{10} - 2f_{12}f'_{12}f'_{10} + 2 f_{12}f_{13}f_{20}f_{10} - f_{10}f_{12}f''_{12}$$

The remaining three coefficients are obtained in a straigt forward manner. Since they are not used in following derivation and are rather involved they are not given here. The f_{ij} are all functions of y and are defined following (4.22) - (4.23).

A solution of the form

$$\Sigma F_n \gamma^{-n} \exp(i\gamma\xi(y))$$

is assumed. Substituting this into (4.26) yields to highest order

$$\xi'(y) = \left[(g_{26} \pm \Delta(y) / (2g_{44}) \right]^{\frac{1}{2}} \qquad (4.27)$$

where

$$\Delta(y) = (g_{26} - 4g_{44}g_{08})^{\frac{1}{2}}$$

Let $\xi_1'(y)$ denote the positive branch of (4.27) and $\xi_2'(y)$ the negative branch. As expected

$$\lambda_i = \xi_i'(0)\gamma \quad ; \quad \lambda_i' = \xi_i'(1)\gamma \quad i = 1,2$$

Within the frontal region

$$V_1(y;\gamma) = \sum_{n=0}^{\infty} \left\{ A_n(y)\exp(i\gamma\xi_1(y) + B_n(y)\exp(-i\gamma\xi_1(y)) + C_n(y)\exp(i\gamma\xi_2(y)) + D_n(y)\exp(-i\gamma\xi_2(y)) \right\} \gamma^{-n}$$

The next order differential equations and their solutions are

$$A_0' + K_1(y)A_0 = 0 \quad ; \quad A_0(y) = A_0(0)\exp\left(-\int_0^y K_1 d\zeta\right) \tag{4.28}$$

$$B_0' + K_1(y)B_0 = 0 \quad ; \quad B_0(y) = B_0(1)\exp\left(\int_y^1 K_1 d\zeta\right) \tag{4.29}$$

$$C_0' + K_2(y)C_0 = 0 \quad ; \quad C_0(y) = C_0(0)\exp\left(-\int_0^y K_2 d\zeta\right) \tag{4.30}$$

$$D_0' + K_2(y)D_0 = 0 \quad ; \quad D_0(y) = D_0(1)\exp\left(\int_y^1 K_2 d\zeta\right) \tag{4.31}$$

where

$$K_i(y) = (-1)^{i}\tfrac{1}{2}\left\{ \xi_i''(y)\{g_{26}(y) - 6\xi_i^2(y)g_{44}(y) + 2\xi_i'(y)\{g_{16}(y) - \xi_i'(y)g_{34}(y)\}\right\} / (\xi_i'(y)\Delta(y)) \quad i=1,2$$

To obtain the matching conditions at the edges of the front, it is necessary to first expand the coefficients of the reflected

and transmitted waves in terms of γ, in the following manner

$$B_R = \Sigma\, B_{Rn}\gamma^{-n} \quad ; \quad D_R = \Sigma\, D_{Rn}\gamma^{-n} \quad ; \quad A_T = \Sigma\, A_{Tn}\gamma^{-n} \quad ; \quad C_T = \Sigma\, C_{Tn}\gamma^{-n}$$

Consider first the situation when $C_I = 0$, that is the energy is incident upon the front in one mode only. The matching conditions to highest order are

$$A_0(0) = H_{11}A_I\exp(-i\gamma\xi_1(0))$$

$$B_0(0) = H_{11}B_{R0}\exp(i\gamma\xi_1(0))$$

$$C_0(0) = 0$$

$$D_0(0) = H_{11}D_{R0}\exp(i\gamma\xi_2(0))$$

$$A_0(1) = H_{11}A_{T0}\exp(-i\gamma\xi_1(1))$$

$$B_0(1) = 0$$

$$C_0(1) = H_{11}C_{T0}\exp(-i\gamma\xi_2(1))$$

$$D_0(1) = 0$$

The application of the matching conditions to the solutions (4.28) - (4.31) yields

$$B_0(y) = 0 \quad ; \quad C_0(y) = 0 \quad ; \quad D_0(y) = 0$$

and thus

$$B_{R0} = 0 \quad ; \quad C_{T0} = 0 \quad ; \quad D_{R0} = 0$$

The next order differential equations for B_1, C_1 and D_1 are the same as for B_0, C_0 and D_0, respectively. The differential equation for A_1 differs and

is given below

$$A_1' + K_1(y)A_1 = -\tfrac{1}{2}\{\xi_1'\Delta\}^{-1}\Big[\{g_{26}-6\xi_1'^2 g_{44}\}A_0'' + 2\{g_{16}+3\xi_1'^2 g_{34}-12\xi_1''\xi_1' g_{44}\}A_0'$$
$$+\{g_{06}-\xi_1'^2 g_{24}+6\xi_1'\xi_1'' g_{34}+\xi_1'^4 g_{42}-4\xi_1'''\xi_1' g_{44}-3\xi_1''^2 g_{44}\}A_0\Big] \qquad (4.32)$$

Since the mean velocities (u_1 and u_2) are both zero a at the edges of the front, then

$$\xi_i''(0) = 0 \quad ; \quad \xi_i''(1) = 0 \qquad \text{for } i = 1,2$$

$$K_i(0) = 0 \quad ; \quad K_i(1) = 0 \qquad \text{for } i = 1,2$$

and

$$A_0'(0) = 0 \quad ; \quad A_1'(1) = 0$$

Utilizing these, the appropriate boundary conditions are

$$A_1(0) = 0$$

$$B_1(0) = H_{11}B_{R1}\exp(i\gamma\xi_1(0))$$

$$C_1(0) = 0$$

$$D_1(0) = H_{11}D_{R1}\exp(i\gamma\xi_2(0))$$

$$A_1(1) = H_{11}A_{T1}\exp(-i\gamma\xi_1(1))$$

$$B_1(1) = 0$$

$$C_1(1) = H_{11}C_{T1}\exp(-i\gamma\xi_2(1))$$

$$D_1(1) = 0$$

Application of these conditions to the differential equations, gives

$$B_1(y) = 0 \quad ; \quad C_1(y) = 0 \quad ; \quad D_1(y) = 0$$

and so

$$B_{R1} = 0 \quad ; \quad C_{T1} = 0 \quad ; \quad D_{R1} = 0$$

This is not unexpected, since this behavior is found in the WKB expansion for the two layer model.

The next order equations for B_2, C_2 and D_2 are once again the same as for B_0, C_0 and D_0, respectively. The matching conditions are such that this time there is a non-zero reflection coefficient. It is interesting to note, however, that if u_{1y} and u_{2y} are zero at $y = 0$ and $y = 1$, then once again there would be no energy scattered into the other modes, nor any reflected in the same mode. That is to say, all the energy would be transmitted in the same mode.

Consider the matching conditions for $B_2(y)$

$$B_2(0) = H_{11}B_{R2}\exp(i\gamma\xi_1(0)) + \left[iQ_1(0)A_1'(0)+Q_2(0)A_0''(0)+Q_3(0)A_0(0)\right]\exp(2i\gamma\xi_1(0))$$

$$B_2(1) = \left[iQ_1(1)A_1'(1)+Q_2(1)A_0''(1)+Q_3(1)A_0(1)\right]\exp(2i\gamma\xi_1(1))$$

where

$$Q_1(y) = -\tfrac{1}{2}\xi_1'^{-1}(y) \qquad y = 0,1$$

$$Q_2(y) = -g_{44}(y)/\Delta(y) \qquad y = 0,1$$

$$Q_3(y) = -\tfrac{1}{2}\xi_1'''(y) \qquad y = 0,1$$

It is necessary to use several other relationships to calculate the reflection coefficient. When evaluated

at $y = 0$ and $y = 1$ (4.32) becomes

$$A_1'(y) = i(S_1(y)A_0''(y) + S_2(y)A_0(y)) \qquad y = 0,1$$

where

$$S_1(y) = -\tfrac{1}{2}\{g_{26}(y)-6\xi_1'^2(y)g_{44}(y)\}/(\xi_1'(y)\Delta(y))$$

$$S_2(y) = -\tfrac{1}{2}\{g_{06}(y)-\xi_1'^2(y)g_{24}(y)-\xi_1'''(y)g_{44}(y)\}/(\xi_1'(y)\Delta(y))$$

If we also differentiate (4.28) and evaluate the resulting equation at $y = 0$ and $y = 1$, then

$$A_0'' = -K_1'A_0$$

Finally noting that

$$A_0(1) = H_{11}A_I\exp(-i\gamma\xi_1(0))\exp(-\int_0^1 K_1(y)dy)$$

we have

$$\left|\frac{B_R}{A_I}\right| = \gamma^{-2}\left|F(0) - F(1)\exp(2i\gamma(\xi_1(1)-\xi_1(0))\right| + o(\gamma^{-3}) \qquad (4.25)$$

where

$$F(y) = Q_3(y) - Q_1(y)S_2(y) + \{Q_1(y)S_1(y)-Q_2(y)\}K_1'(y)$$

The coefficients R_2 and T_2 also decay as γ^{-2} and are explicitly given in Appendix B. The other transmission coefficient T_1 is determined by the use of (4.25). The case of the alternate mode being incident ($A_I = 0$) gives similar results.

While the resulting equations are unwieldy, they do yield information that for wavelengths much less than the across front distance virtually all the energy in a wave is transmitted in the same mode. If we

consider a four layer model, the results for high wavenumber are similar. When WKB perturbation solution is obtained, the highest order matching conditions are once again homogeneous at $y = 1$ for all the reflected waves, and at $y = 0$ for the transmitted waves in the modes in which no energy is incident upon the front. Thus, the energy is reflected or scattered to other modes goes as γ^{-2} for large non-dimensional wavenumber. The requirement that the steady state velocities are zero at each edge of the front forces the next order matching conditions for the reflected and scattered waves to be homogeneous at one edge of the front also and thus there is no energy in the these reflected or scattered waves either. Therefore, as in the two and three layer models, the energy reflected or scattered is proportional to γ^{-4} for high wavenumbers.

It is unfortunate that an analytic perturbation solution for low wavenumber is not possible. If $\gamma \to 0$, the lowest order equations (from (4.22) and (4.23)) are still second order, coupled differential equations, which do no lend themselves to an analytic solution easily. The transmission and reflection properties for low wavenumbers are rather complex.

Not only is there a dependence upon the depth of the various layers, but also on the ratio of the change in density between the layers. The problem is well behaved in the limiting cases. If D is very small (less than .05) or very large (greater than 20) the problem collapses to a two layer model. Also, as any of the layer depths approach zero, the results approximate a two layer model.

The physical characteristics of the model that we have defined, is seen in the Gulf Stream. The isopycnals tilt upward at an approximate slope of 1:100 (Kao, 1980) to form the front, which separates the denser slope water from the warmer, less dense water of the Sargoasso Sea. Associated with the sloping pycnocline is an approximatly geostrophic current flowing along the front. From typical hydrographic sections of the Gulf Stream (Stommel, 1965, p. 45-51, and Fuglister, 1963) it can be seen that the isopycnals tilt upward with approximately the same slope. The ratio of the changes in density, D, appear to be less than 1 (that is the difference in density between the top two layers is greater than or equal to the change in the density between the lower layers).

As in the two layer case, the depths of the layers in the frontal region are defined with polynomials.

$$h_1(y) = 1-\alpha_1(3y^2-2y^3)$$

$$h_2(y) = 1-\alpha_2(3y^2-2y^3)$$

$$h_3(y) = 1-\alpha_3(3y^2-2y^3)$$

$$h_5(y) = 1+\alpha_4(3y^2-2y^3)$$

where

$$\alpha_1 = (H_{11}-H_{12})/H_{11}$$

$$\alpha_2 = (H_{21}-H_{22})/H_{21}$$

$$\alpha_3 = (H_{31}-H_{32})/H_{31}$$

$$\alpha_4 = (H_{11}-H_{12})/(H_{21}+H_{31})$$

Defining the depths of the layers in this way lets the steady state velocities be zero at both edges of the front. Using these equations we obtain the reflection and transmission coefficient numerically using the method described in Appendix A. Three different frontal structures are examined here.

The first (Figure 20a,b,c) is simple if not physically appropriate to the Gulf Stream. Figure 20a displays the vertical modal structure as defined in Section 3.2. Only the upper boundary between the layers tilts upwards, while the depth of the lower layer remains constant. What is called the first

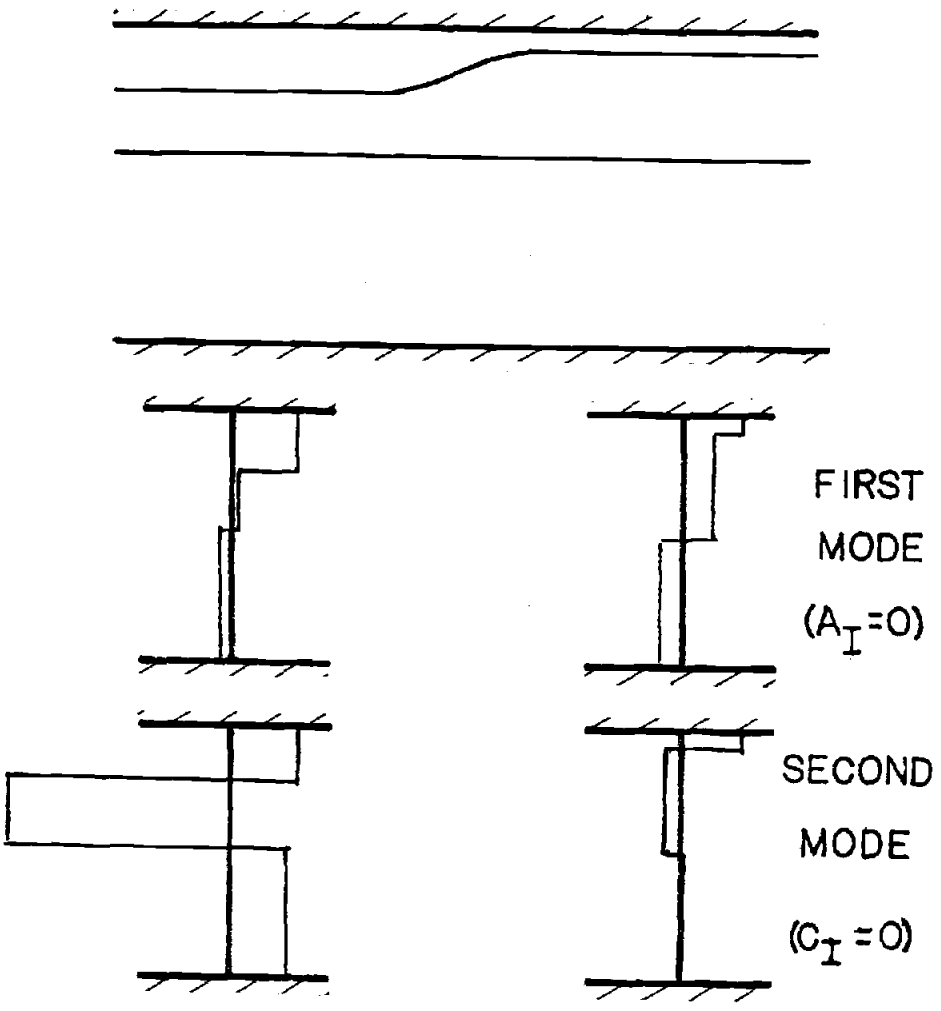

Figure 20a: Using the parameters $\alpha_1 = \alpha_2 = .8$, $\alpha_3 = 0.$, $\alpha_4 = .11$, and D = .6, the frontal depth profile and the vertical modal structure are displayed.

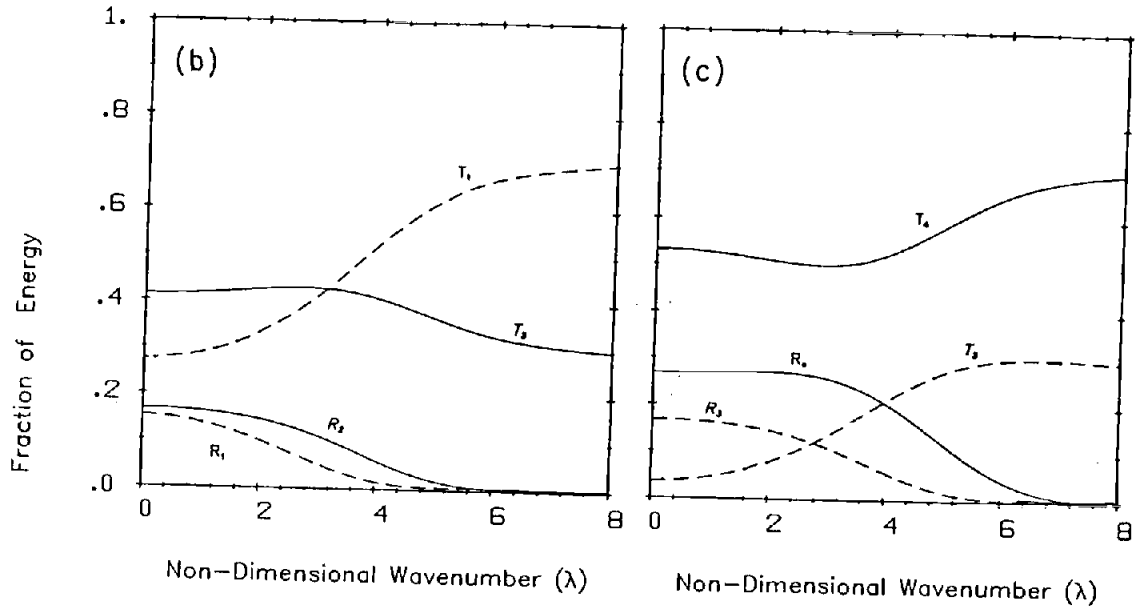

Figure 20b: Fraction of energy reflected (R_1) and transmitted (T_1) in the same mode and the scattered reflected (R_2) and the scattered transmitted energy (T_2). The second mode is incident (C_I=0). 20c: Fraction of energy reflected (R_4) and transmitted (T_4) in the same mode, and the scattered reflected energy (R_3) and the scattered transmitted energy (T_3). The first mode is incident (A_I=0).

has a vertical structure that goes through zero only once while the second mode passes through it twice. The parameters (α_i) that determine the shape of the front are listed in the caption. The reflected and transmitted quantities shown in figure 20b, are the results when the second mode is incident upon the front and those in figure 20c are the results when the first mode is incident. It is expected that the first mode will not "see" the front as much as the second mode since the change in the velocity between the upper two layers is less for mode 1 than for mode 2. This is indeed the case. The transmission energy transmitted through the front (T_4) in the same mode is over 50% in figure 20c, while only about 25% in 20b. This, of course, only applies to the small wavenumber case. For high wavenumbers, the scattered and reflected energies go to zero an and thus almost all the energy would be transmitted in the same mode. In both 20b and 20c the reflected energies go to zero at high wavenumbers faster than the scattered transmitted energy. This is an artifact of the frontal shape, and if the figures were expanded to higher wavenumbers the scattered transmitted energies would be less than the reflected energies.

The only differnce between figure 21 a,b,c and 22 a,b,c is the value of D. For figure 21, D = .5 and for 22, D = .2. There is similarity between shapes of various reflected and transmitted energies but their amplitudes at low wavenumber are considerable different. Since D is greater in 21 than 22 this imples that the change in density across the upper two layers relative to the change across the lower two is greater for the front in figure 22 than 21. Thus it is expected that the first mode will transmitted through the front unchanged more so in 21 than in 22. This is indeed the case. For higher wavenumbers virtually all the energy is transmitted through the front unchanged as expected from the WKB approximation. It is unfortunate that no low wavenumber solution is obtained, since it is only in this region that that front has an appreciable effect upon the wavefield.

The major result here is that for low wavenumbers that a considerable amount of the energy of any wave is scattered into other modes. To better understand the where the energy would be scattered it is necessary to have at least one more layer. This is not feasible at this time.

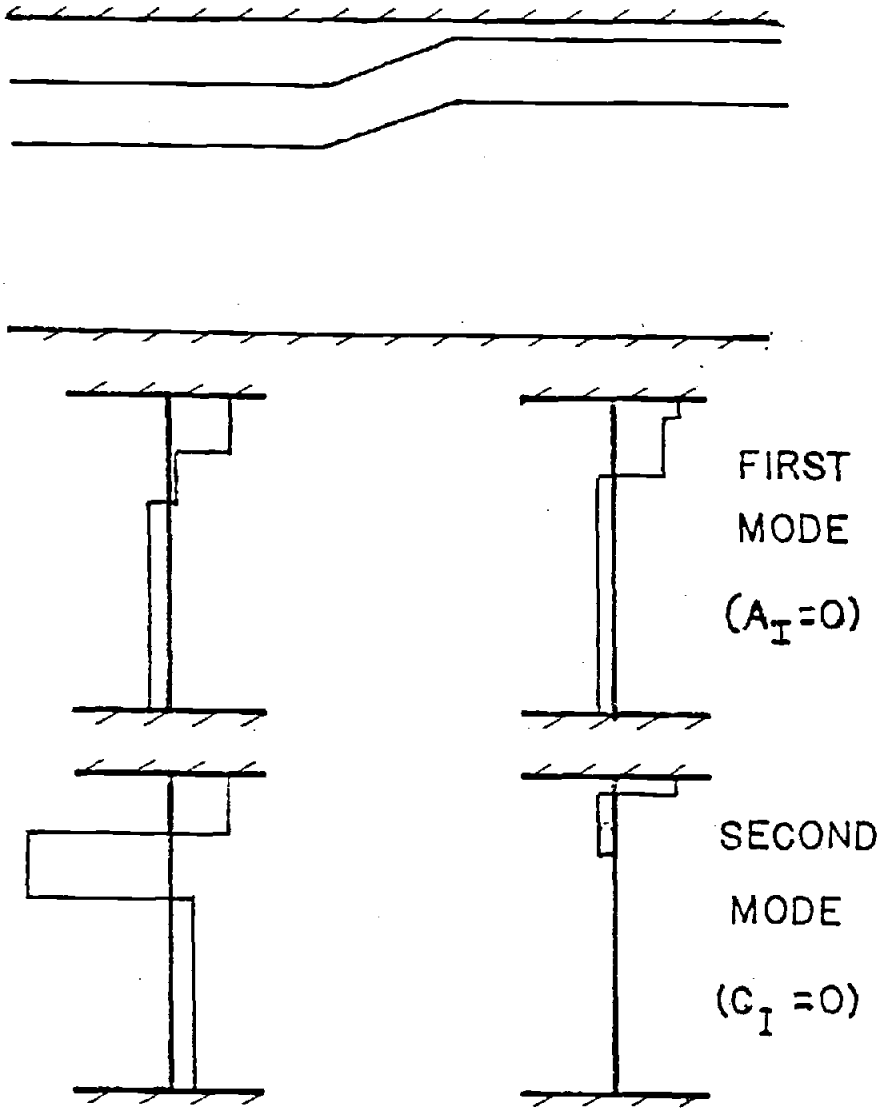

Figure 21a: Using the parameters α_1=.8, α_2=0, α_3=.13, α_4=.11, and D=.5, the frontal depth profile and the vertical modal structure are displayed.

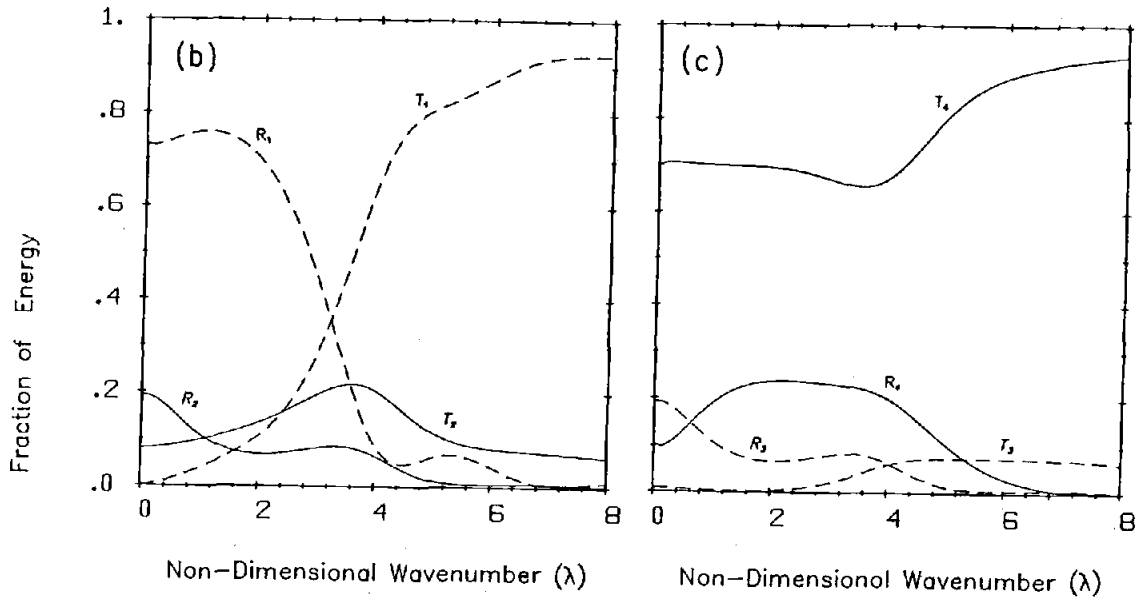

Figure 21 b: The labels on the plots are the same as defined in 20b.

21c: The labels on the plots are the same as defined in 20c.

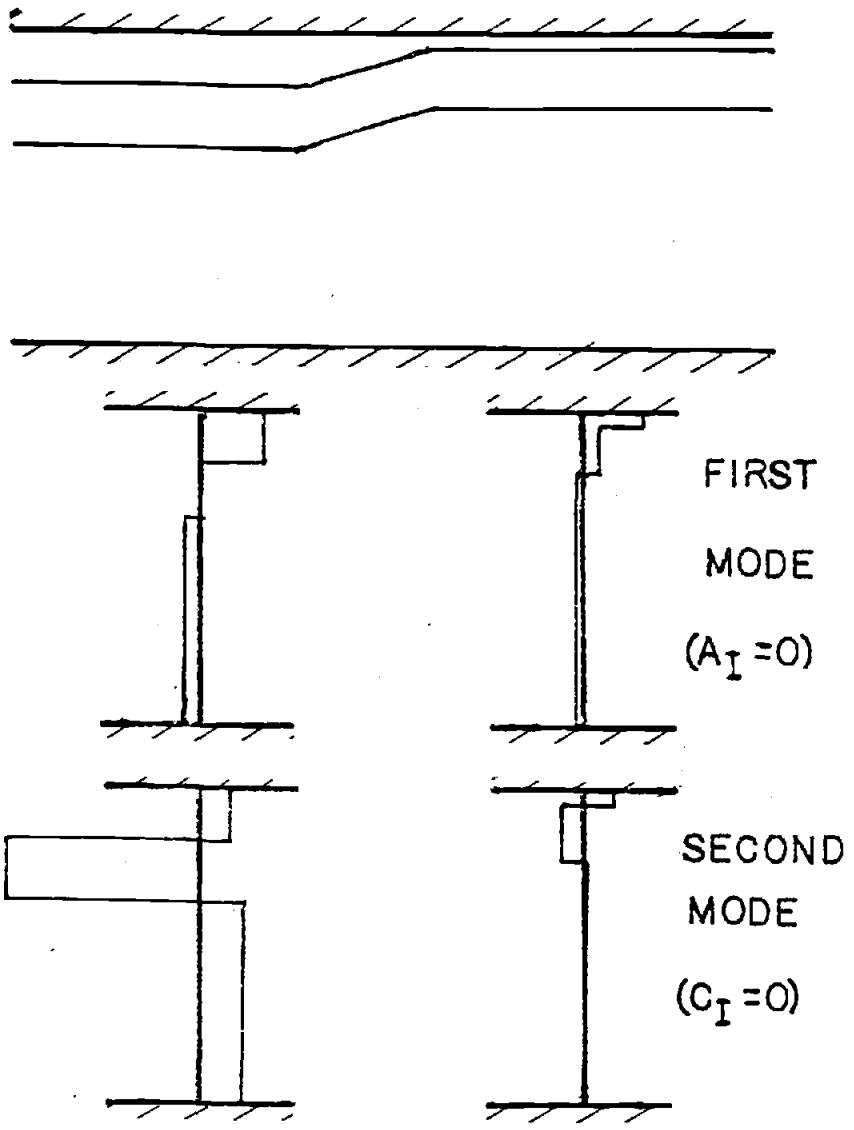

Figure 22a: Using the same frontal depth parameters (α_i) as in figure 21 and D = .2, the frontal depth profile and the vertical modal structure are displayed.

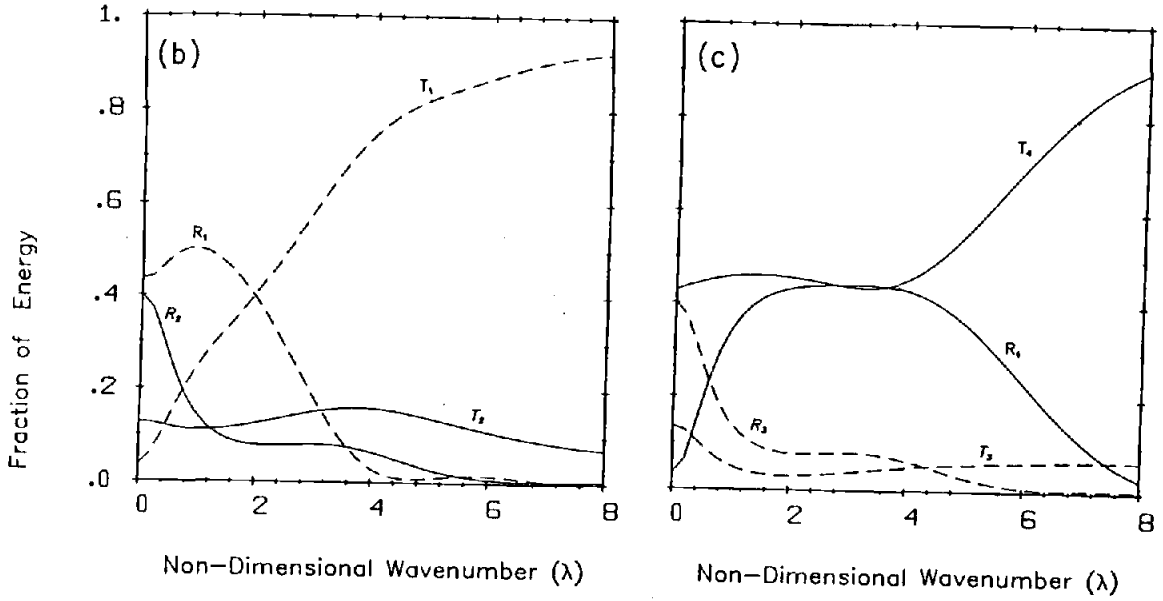

Figure 22 b: The labels on the plots are the same as defined in 20b.

22c: The labels on the plots are the same as defined in 20c.

V SUMMARY AND CONCLUSIONS

The influence of a frontal structure with its accompanying horizontally sheared, geostrophic velocity upon an internal wave field is investigated in a theoretical model. A portion of the energy of any wave that propagates at right angles to the front is reflected while the remainder is transmitted. For high wavenumbers (waves whose wavelength is much less than the width of the front) the frontal structure has a minimal effect on the wave as it propagates through the front. In a two layer model only a small part of the wave energy is reflected. Even for waves whose wavelength is equal to the frontal width, less than one percent of the energy is reflected and as the wavenumber (λ) increases the amount of reflection decreases as λ^{-4}. Similarly, for a model with more than two layers, only a small part of the energy is scattered into the other vertical modes. For low wavenumbers (those waves whose wavelength is greater than the frontal width) this is definitely not the case. Much of the energy of these waves is reflected, if the relative depth change of the upper layer is sufficiently large. Similarly, if there is more than

one baroclinic mode most of the energy of these long waves is scattered into the other vertical modes or reflected in the same mode.

For non-normal incidence the situation becomes more complex. First consider a frontal structure that does not allow any critical layers. Along a curve of constant frequency, as the angle of incidence approaches ±90°, the reflection coefficient approaches one - total reflection. For frequencies close to the inertial, the maximum transmission occurs at near normal incidence. As curves of higher frequencies are considered, the angle of incidence at which minimum reflection occurs deviates further and further from normal incidence. This trend is the result of the phase speed decreasing and becoming closer in magnitude to the maximum mean geostrophic speed.

A sufficiently strong front permits the occurrence of critical layers. For the vertically propagating internal wave discussed in LeBlond and Mysak (1978) the mean flow absorbs energy from the internal wave. This is not the case for these internal waves which propagate through horizontal shear. both over-reflection and under-reflection occur. In the examples

computed in section 3.6 over reflection was the most common behavior, and so is a source of energy for the internal wavefield.

While evidence in the ocean of the reflection properties of a wave may not be easily obtainable, there is some evidence of the transfer of energy from a mesoscale horizontal velocity shear to the internal wave field as is seen in data analyzed by Brown and Owens (1981). The Reynolds stress is used to show this. As derived in chapter 3, Reynolds stress is invariant in the cross front direction if there is no critical layer. When they do occur this is not true. The low mean speed (25 cm s^{-1}) requires that a higher order vertical mode (with a lower phase speed) be involved in the formation of the critical layer. There are other possible mechanisms in addition to the occurrence of critical layers that could explain this transfer of energy as discussed in their paper. Other evidence is from the study of the north Pacific subtropical front, where there is an intensification of the low frequency wave energy at the edge of the front (where the upper layer is

deepest)(Paulson and Niiler, 1981). However, as in the other example, the low speeds of the accompanying geostrophic velocity (40 cm s^{-1}) (Roden, 1981) indicates the involvement of higher vertical modes. Therefore, specific comments are difficult to infer, since the two layer model has only one vertical baroclinic mode. It is necessary to examine each problem separately and develop a model specifically fitted to the physical parameters of the situation. The lack of any analytic result for the behavior of internal waves about a critical layer does not permit generalizations.

While the methods of solution are straightforward the computational time on a computer would be too extensive for a three or more layer model with non-normal incidence to be developed.

BIBLIOGRAPHY

Acton, Forman S., 1970: Numerical Methods that Work Harper & Row, N.Y., 591 pp.

Brown, Ellen D. and W. Brechner Owens, 1981: Observations of the Horizontal Interactions between the Internal Wave Field and the Mesoscale Flow. J. Phys. Oceanogr., 11:1474-1480.

Jones, Walter L., 1967: Propagation of internal gravity waves in fluids with shear flow and rotation. J. Fluid Mech., 30:439-448.

LeBlond, P.H. and L.A. Mysak, 1978: Waves in the Ocean, Elsevier Scientific Publishing Co., Amsterdam, 602 pp.

Lindzen, R.S. and H.L. Kuo, 1969: A reliable method for the numerical integration of a large class of ordinary and partial differential equations. Monthly Weather Review, 97:732-734.

Nayfeh, Ali Hasan, 1973: Perturbation Methods. John Wiley & Sons, N.Y., 425 pp.

Paulson, C.A. and P.P. Niiler, 1981: FRONTS 80: Preliminary Results From an Investigation of the Wintertime North Pacific Subtropical Front. OSU Publication, Ref. no. 81-2.

Olbers, Dirk J., 1981: A formal theory of Internal Wave Scattering with Applications to Ocean Fronts. J. of Phys. Oceanogr., 11:1078-1099.

Roden, Gunnar I, 1981: Mesoscale Thermohaline, Sound Velocity and Baroclinic Flow Structure of the Pacific Subtropical Front During the Winter of 1980. J. of Phys. Oceanogr., 11:658-675.

Sears, M., 1963: Progress in Oceanography. Vol. 1, The Macmillian Co., M. Sears Editor, 383 pp.

Stommel, Henry, 1958: The Gulf Stream. Univ. of Calif. Press and Cambridge Univ. press, 202 pp.

Wasow, Wolfgang, 1965: Asymptotic Expansion for Ordinary Differential Equations. Pure and Applied Mathematics, Vol. XIV., John Wiley and Sons, N.Y., 349 pp.

Worthington, L.V., 1976: On the North Atlantic Circulation. The John Hopkins Univ. Press, 110 pp.

APPENDICES

APPENDIX A

The method of diagonalizing the matrix and thus numerically solving the differential equations for the two and three layer normal incidence case is adapted from Lindzen and Kuo (1969).

First consider the two layer model (chapter 2). The equation of the form

$$V_{yy} + h(y)V = 0 \qquad \text{(A1)}$$

with

$$V_y - i\lambda V = -2i\lambda B_R H_{11} \qquad y = 0 \qquad \text{(A2)}$$

$$V_y + i\lambda V = 2i\lambda H_{11} A_I \qquad y = 0 \qquad \text{(A3)}$$

$$V_y - i\lambda' V = 0 \qquad y = 0 \qquad \text{(A4)}$$

Equation A1 can be written finite difference form

$$A\,V_{n-1} + B_n V_n + A V_{n+1} = 0 \qquad n = 1,2,..,N-1$$

where

$$A = 1/(\delta y)^2 = N^2$$

$$B_n = -2/(\delta y)^2 + h(y_n) \qquad y_n = n\,\delta y$$

The boundary conditions can be expressed in finite differnce form as

$$-(N+i\lambda)V_0 + NV_1 = -2i\lambda H_{11} B_R \qquad \text{(A5)}$$

$$-(N-i\lambda)V_0 + NV_1 = 2i\lambda H_{11} A_I \qquad \text{(A6)}$$

$$-NV_{N-1} + (N-i\lambda')V_N = 0 \qquad \text{(A7)}$$

Then following Lindzen and Kuo, and using (A5) and (A7)

$$\alpha_{a0} = (N+i\lambda)^{-1}N$$

$$\beta'_{A0} = -(n+I\lambda)^{-1}2i\lambda H_{11}$$

$$\beta_{A0} = \beta'_{A0}\, A_I$$

$$\alpha_{An} = -(A\alpha_{A,n-1} + B_n)^{-1}A$$

$$\beta'_{A,n} = -(A\alpha_{A,n-1} + B_n)^{-1}A\beta'_{A,n-1}$$

$$\beta_{A,n} = \beta'_{A,n}\ A_I$$

Thus we finally have

$$V_N = (N-i\lambda'-\alpha_{A,N-1}N)^{-1}N\beta'_{A,N-1}\ A_I \qquad (A8)$$

If we use (A6) and (A7) as the boundary conditions then it is clear that

$$\alpha_{B,n} = \alpha^*_{A,n} \quad ; \quad \beta'_{B,n} = \beta'^*_{A,n}$$

where * denotes the complex conjugate. The second relationship is

$$V_N = (N-i\lambda'-\alpha^*_{A,N-1}N)^{-1}N\beta'^*_{A,N-1}B_R \qquad (A9)$$

and so from (A8) and (A9)

$$\left|\frac{B_R}{A_I}\right| = \left|\frac{N-i\lambda'-N\alpha^*_{A,N-1}}{N-i\lambda'-N\alpha_{A,N-1}}\right| \qquad (A10)$$

The three layer model is a bit more complicated since it entails matrix manipulations, but is essentially the same in theory. Let

$$\underset{\sim}{F} = \begin{vmatrix} V_1 \\ V_2 \end{vmatrix}$$

then

$$\frac{d}{dy^2}\underset{\sim}{F} + \underset{\approx}{S}(y)\underset{\sim}{F} = 0$$

where

$$\underset{\sim}{S}(y) = \begin{vmatrix} g_1(y) & -g_2(y) \\ -g_4(y) & g_3(y) \end{vmatrix}$$

In the finite differnce form we have

$$\underset{\sim}{\underset{\sim}{A}}F_{n-1} + \underset{\sim}{\underset{\sim}{B}}_n F_n + \underset{\sim}{\underset{\sim}{A}}F_{n+1} = 0$$

where

$$\underset{\sim}{\underset{\sim}{A}} = N^2\underset{\approx}{I} \qquad \underset{\sim}{\underset{\sim}{B}} = \underset{\sim}{\underset{\sim}{S}}(y_n) - 2\underset{\sim}{\underset{\sim}{A}}$$

Here $\underset{\approx}{I}$ is the identity matrix. The matching conditions can be expressed as

$$\underset{\sim}{\underset{\sim}{D}}_1 F_y + \underset{\sim}{\underset{\sim}{E}}_1 F = \underset{\sim}{\underset{\sim}{R}}_1 \begin{bmatrix} A_I \\ C_I \end{bmatrix} \tag{A10}$$

$$\underset{\sim}{\underset{\sim}{D}}^*_1 F_y + \underset{\sim}{\underset{\sim}{E}}_1 F = \underset{\sim}{\underset{\sim}{R}}^*_1 \begin{bmatrix} B_R \\ D_R \end{bmatrix} \tag{A11}$$

$$\underset{\sim}{\underset{\sim}{D}}_2 F_y + \underset{\sim}{\underset{\sim}{E}}_2 F = \underset{\sim}{\underset{\sim}{R}}_2 \begin{bmatrix} A_T \\ C_T \end{bmatrix} \tag{A12}$$

$$\underset{\sim}{\underset{\sim}{D}}^*_2 F_y + \underset{\sim}{\underset{\sim}{E}}_2 F = 0 \tag{A13}$$

They can be written in finite difference form as

$$(\underset{\sim}{E}_1 - \underset{\sim}{ND}_1)\underset{\sim}{F}_0 + \underset{\sim}{ND}_1\underset{\sim}{F}_1 = \underset{\sim}{R}_1 \begin{bmatrix} A_I \\ C_I \end{bmatrix}$$

$$(\underset{\sim}{E}_1 - \underset{\sim}{ND}_1)^*\underset{\sim}{F}_0 + (\underset{\sim}{ND}_1)^*\underset{\sim}{F}_1 = \underset{\sim}{R}^*_1 \begin{bmatrix} B_R \\ D_R \end{bmatrix}$$

$$-(\underset{\sim}{ND}_2)\underset{\sim}{F}_{N-1} + (\underset{\sim}{ND}_2 + \underset{\sim}{E}_2)\underset{\sim}{F}_N = \underset{\sim}{R}_2 \begin{bmatrix} A_T \\ C_T \end{bmatrix}$$

$$-(\underset{\sim}{ND}_2)^*\underset{\sim}{F}_{N-1} + (\underset{\sim}{ND}_2 + \underset{\sim}{E}_2)^*\underset{\sim}{F}_N = \begin{bmatrix} 0 \\ 0 \end{bmatrix}$$

We now calculate a series of matrixes utilizing (A10) as follows

$$\underset{\sim}{\alpha}_{A0} = -(\underset{\sim}{E}_1 - \underset{\sim}{ND}_1)^{-1}\underset{\sim}{ND}_1$$

$$\underset{\sim}{\beta}'_{A0} = (\underset{\sim}{E}_1 - \underset{\sim}{ND}_1)^{-1}\underset{\sim}{R}_1$$

$$\underset{\sim}{\beta}_{A0} = \underset{\sim}{\beta}'_{A0}\begin{vmatrix} A_I \\ C_I \end{vmatrix}$$

$$\underset{\sim}{\alpha}_{An} = -(\underset{\sim\sim}{A}\underset{\sim}{\alpha}_{A,n-1} + \underset{\sim}{B}_n)^{-1}\underset{\sim}{A}$$

$$\underset{\sim}{\beta}'_{An} = -(\underset{\sim\sim}{A}\underset{\sim}{\alpha}_{A,n-1} + \underset{\sim}{B}_n)^{-1}\underset{\sim\sim}{A}\underset{\sim}{\beta}'_{A,n-1}$$

$$\underset{\sim}{\beta}_{An} = \underset{\sim}{\beta}'_{An}[\, A_I \,,\, C_{,} \,]^T$$

Thus utilizing

Thus utilizing (A12)

$$\underset{\sim}{F}_{1N} = (N\underset{\sim}{D}_2+\underset{\sim}{E}_2-N\underset{\sim}{D}_2\underset{\sim}{\alpha}_{A,N-1})^{-1}\left(\underset{\sim}{R}_2\begin{vmatrix}A_T\\C_T\end{vmatrix}+N\underset{\sim}{D}_2\underset{\sim}{\beta}'_{A,N-1}\begin{vmatrix}A_I\\C_I\end{vmatrix}\right)$$

$$= \underset{\sim}{Q}_1\begin{vmatrix}A_T\\C_T\end{vmatrix} + \underset{\sim}{Q}_2\begin{vmatrix}A_I\\C_I\end{vmatrix}$$

Utilizing (A13), we have

$$\underset{\sim}{F}_{2N} = (N\underset{\sim}{D}^*_2+\underset{\sim}{E}^*_2-N\underset{\sim}{D}^*_2\underset{\sim}{\alpha}_{A,N-1})^{-1}\left(N\underset{\sim}{D}^*_2\underset{\sim}{\beta}'_{A-N-1}\begin{vmatrix}A_I\\C_I\end{vmatrix}\right.$$

$$= \underset{\sim}{Q}_3\begin{vmatrix}A_I\\C_I\end{vmatrix}$$

Equations (A11) and (A13) yield the third relationship

$$\underset{\sim}{F}_{3N} = (N\underset{\sim}{D}^*_2+\underset{\sim}{E}^*_2-N\underset{\sim}{D}^*_2\underset{\sim}{\alpha}^*_{A,N-1})^{-1}N\underset{\sim}{D}_2\underset{\sim}{\beta}'^*_{A,N-1}\begin{vmatrix}B_R\\D_R\end{vmatrix}$$

$$= \underset{\sim}{Q}_4\begin{vmatrix}B_R\\D_R\end{vmatrix}$$

Finally $\underset{\sim}{F}_{1N} = \underset{\sim}{F}_{2N}$ and $\underset{\sim}{F}_{2N} = \underset{\sim}{F}_{3N}$ so there are now four equations and 6 unknowns ($A_I, C_I, B_R, D_R, A_T, C_T$). It is straight forward to caluclate the reflection and transmission coefficients by letting either

$C_I = 0$ or $A_I = 0$.

$$\left|\frac{C_{T_2}}{A_I}\right| = \frac{1}{\gamma^2}\Big|[(R_3(0)-R_1(0)S_2(0)+(R_1(0)S_1(0)-R_2(0))K_1'(0)]$$

$$\exp(-\int_0^{'}K_2(y)dy)-[R_y(1)-R_1(1)S_2(1)$$

$$+ (R_1(1)S_1(1)-R_2(1)\ K_1'(1)]\exp(-\int_0^{'}K_1(y)dy)$$

$$\exp((\xi_1(1)-\xi_2(1)-\xi_2(0))i\gamma_{\ })\Big|$$

$$R_1(y) = -g_{44}\{\xi_1'^2 + \xi_2'\xi_2'\}(\xi_2'\Delta)^{-1}$$

$$R_2(y)= -\tfrac{1}{2}(3\xi_1' + \xi_2')g_{44}(\xi_2')\Delta)^{-1}$$

$$R_3(y) = -\tfrac{1}{2}g_{44}(\xi_1''' - (H_{21}h_1^{-1} - \frac{H_{11}+H_{21}}{H_{11}}\ \xi_1'^2)u_{2y}$$

$$+ u_{1y}h_1^{-1})(\xi_1' + \xi_2')(\xi_2'\Delta)^{-1}$$

$$\left|\frac{D_R}{A_I}\right| = \frac{1}{\gamma^2}\Big|F(0)\exp\Big(-\int_0^1 K_2(y)\Big)$$

$$-F(1)\exp\Big(-\int_0^1 K_1(y)dy\Big)$$

$$\exp\big((\xi_1(1)+\xi_2(1)-2\xi_1(0))i\gamma$$

$$F(y) = R_3(y)-R_1(y)S_2(y)+(R_1(y)S_1(y)-R_2(y))K_1'(y)$$

where

$$R_1 = -g_{44}'(\xi_1'\xi_2' - \xi_1'^2)(\xi_2'\Delta)^{-1}$$

$$R_2 = +\tfrac{1}{2}g_{44}'(3\xi_1' - \xi_2')(\xi_2'\Delta)^{-1}$$

$$R_3 = \tfrac{1}{2}g_{44}(\xi_1''' - (H_{21}h_1^{-1} - \frac{H_{11}+H_{21}}{H_{11}}\xi_1'^2)U_{2y}+U_{1y}h_1^{-1})$$

$$(\xi_1' - \xi_2')(\xi_2'\Delta)^{-1}$$

Appendix C

Consider the system of equations

$$\underset{\sim}{\phi}_y = \underset{\approx}{A}\ \underset{\sim}{\phi}$$

where $\underset{\approx}{A}$ is a 4x4 matrix and $\underset{\sim}{\phi}$ is a vector. Along with this equation are the appropriate matching conditions.

$$\underset{\sim}{\phi}(0) = -\underset{\approx}{A}\begin{pmatrix} B_R \\ D \end{pmatrix} + \underset{\approx}{B}A_I$$

$$\underset{\sim}{\phi}(1) = \underset{\approx}{C}\begin{pmatrix} B_R \\ D' \end{pmatrix}$$

where $\underset{\approx}{A}$ and $\underset{\approx}{C}$ are 4x2 matrices and $\underset{\sim}{B}$ a vector.

Let $\underset{\sim}{\phi}_1(y)$ be the solution to the system of equations if $A_T = 1$ and $D' = 0$ and the system is integrated from $y = 1$ to $y = 0$. Similarly let $\underset{\sim}{\phi}_2(y)$ be the solution if $A_T = 0$ and $D' = 1$. Then

$$\underset{\sim}{\phi} = [\underset{\sim}{\phi}_1 , \underset{\sim}{\phi}_2]\begin{pmatrix} A_T \\ D' \end{pmatrix} = \underset{\approx}{D}\begin{pmatrix} A_T \\ D' \end{pmatrix}$$

Thus

$$\underset{\approx}{A}\begin{pmatrix} B_R \\ D \end{pmatrix} + \underset{\approx}{D}\begin{pmatrix} A_T \\ D' \end{pmatrix} = \underset{\sim}{B}\ A_I$$

or

$$\underset{\sim}{\xi} \begin{pmatrix} B_R \\ D \\ A_T \\ D' \end{pmatrix} = \underset{\sim}{B} A_I$$

and so by inverting $\underset{\sim}{\xi}$ we have the desired relationship.